Energy and exergy analysis of two novel hybrid solar photovoltaic geothermal energy systems incorporating a building integrated photovoltaic thermal system and an earth air heat exchanger system

Masoud Afrand[1,2], Amin Shahsavar[3], Pouyan Talebizadeh Sardari[4], Kamaruzzaman Sopian[5,*], Hamzeh Salehipour[6]

[1]Laboratory of Magnetism and Magnetic Materials, Advanced Institute of Materials Science, Ton Duc Thang University, Ho Chi Minh City, Vietnam

[2]Faculty of Applied Sciences, Ton Duc Thang University, Ho Chi Minh City, Vietnam

[3]Department of Mechanical Engineering, Kermanshah University of Technology, Kermanshah, Iran

[4]Faculty of Engineering, University of Nottingham, University Park, Nottingham, United Kingdom

[5] Solar Energy Research Institute, Universiti Kebangsaan Malaysia, Bangi, Malaysia

[6] Department of Mechanical Engineering, Ilam University, Ilam 69315-516, Iran

* Corresponding author

Emails: ksopian@ukm.edu.my; masoud.afrand@tdtu.edu.vn

Abstract

In this paper, two novel configurations of the building integrated photovoltaic thermal (BIPVT)-compound earth-air heat exchanger (EAHE) system are proposed. Both the configurations operate in two modes, namely heating and cooling modes. In the heating mode of the configuration A, the cold outdoor air is twice preheated by passing through the EAHE and BIPVT systems. In the cooling mode of the configuration A, the hot outdoor air is precooled by flowing inside the EAHE system and the PV modules are cooled using the building exhaust air. The cooling mode of the configuration B is similar to the configuration A, while in the heating mode of the configuration B, the outdoor air first enters the BIPVT collector and then passes through the EAHE system. The energetic and exergetic performances of the configurations are investigated for climatic conditions of Kermanshah, Iran. In addition, the impacts of length, width, and depth of air duct located underneath the PV panels, air mass flow rate, length and inner diameter of the pipe of EAHE system on the annual average energetic and exergetic aspects of the best configuration of the BIPVT-EAHE system are evaluated. The outcomes revealed that the annual rate of thermal energy, electrical energy, and thermal exergy captured from the configuration A are respectively 3499.59, 5908.19, and 55.59 kWh, while these values for the configuration B are respectively 3468.16, 5969.87, and 51.76 kWh. In addition, it was found that the configuration A has superior energetic performance than the configuration B, while the overall exergetic performance of the configuration B is higher than the configuration A. Furthermore, it was depicted that both the energetic and exergetic performances of the suggested configurations intensify by augmenting the duct length, duct width, and tube diameter whereas they decline with an increase in the air mass flow rate and duct depth.

Key words: Building integrated photovoltaic thermal (BIPVT); Earth-air heat exchanger (EAHE); Energy; Exergy.

Nomenclature

A	heat exchange surface area of the EAHE system (m^2)
c_p	specific heat capacity of air (J kg^{-1} K^{-1})
$D_{H,BIPVT}$	hydraulic diameter of the BIPVT collector (m)
$D_{i,EAHE}$	inner diameter of the EAHE system (m)
$\dot{E}$	electric power generated by the BIPVT-EAHE system (kWh)
$\dot{E}_{fan,BIPVT}$	electric power consumed by fans to blow air inside the BIPVT collector (kWh)

$\dot{E}_{BIPVT,net}$	net electric power gained from the BIPVT collector (kWh)
$\dot{E}_{EAHE}$	electric power consumption of the EAHE system (kWh)
f_{BIPVT}	fanning friction factor for the BIPVT collector
f_{EAHE}	fanning friction factor for the EAHE system
h	convective heat exchange coefficient of the EAHE system (W K^{-1} m^{-2})
h_c	convective heat exchange coefficient of the BIPVT collector (W K^{-1} m^{-2})
$h_{r,pv-b}$	radiative heat exchange coefficient between the PV modules and back wall (W $K^{-1}m^{-2}$)
$h_{r,pv-s}$	radiative heat exchange coefficient between the PV modules and sky (W $K^{-1}m^{-2}$)
h_w	wind convective heat exchange coefficient (W $K^{-1}m^{-2}$)
I_r	intensity of solar radiation (W m^{-2})
k	thermal conductivity (W m^{-1} K^{-1})
$k_{c,BIPVT}$	loss coefficient of the BIPVT collector
$k_{c,EAHE}$	loss coefficients of the EAHE system
k_{ins}	thermal conductivity of insulation material (W $m^{-1}K^{-1}$)
L	length of the PV duct (m)
L_{EAHE}	Length of the EAHE system (W $m^{-1}K^{-1}$)
$\dot{m}_f$	air mass flow rate (kg s^{-1})
NTU	number of transfer units
ΔP	frictional pressure loss (Pa)
ΔP_{BIPVT}	frictional pressure loss in BIPVT collector (Pa)
ΔP_{EAHE}	frictional pressure loss in EAHE system (Pa)
$\mathrm{PEC_{en}}$	energetic performance evaluation criterion

$\mathrm{PEC_{ex}}$	exergetic performance evaluation criterion
Pr	Prandtl number
$\dot{Q}$	thermal power gained from the BIPVT-EAHE system (kWh)
$\dot{Q}_{BIPVT}$	thermal power gained from the BIPVT collector (kWh)
$\dot{Q}_{EAHE}$	thermal power gained from the EAHE system (kWh)
$\dot{Q}_{EAHE,max}$	maximum possible thermal power gained from the EAHE system (kWh)
Re_{BIPVT}	Reynolds number of the BIPVT collector
Re_{EAHE}	Reynolds number of the EAHE system
S	depth of the PV duct (m)
T_a	outdoor air temperature (K)
T_b	back wall temperature (K)
T_f	air temperature (K)
T_{in}	temperature of inlet air through the PV duct (K)
$T_{in,EAHE}$	temperature of inlet air through the EAHE system (K)
T_{mf}	mean air temperature inside the PV duct (K)
$T_{out,EAHE}$	temperature of outlet air from the EAHE system (K)
T_{pv}	PV module temperature (K)
T_s	sky temperature (K)
T_{soil}	soil temperature (K)
U_b	bottom heat loss coefficient ($\mathrm{W\ K^{-1}m^{-2}}$)
v_w	wind speed ($\mathrm{m\ s^{-1}}$)
W	width of the PV duct (m)
$\dot{X}_{dest,BIPVT}$	exergy loss from the BIPVT collector (kWh)
$\dot{X}_{dest,EAHE}$	exergy loss from the EAHE system (kWh)

$\dot{X}_{el}$	electrical exergy gained from the BIPVT-EAHE system (kWh)
$\dot{X}_{el,BIPVT}$	electrical exergy gained from the BIPVT system (kWh)
$\dot{X}_{el,EAHE}$	electrical exergy gained from the EAHE system (kWh)
$\dot{X}_{el,PV}$	electrical exergy of the PV modules (kWh)
$\dot{X}_{fan,BIPVT}$	exergy of fan consumed power in the BIPVT collector (kWh)
$\dot{X}_{fan,EAHE}$	exergy of fan consumed power in the EAHE system (kWh)
$\dot{X}_{in,BIPVT}$	exergy of air entering the BIPVT collector (kWh)
$\dot{X}_{in,EAHE}$	exergy of air entering the EAHE system (kWh)
$\dot{X}_{out,BIPVT}$	exergy of air leaving the BIPVT collector (kWh)
$\dot{X}_{out,EAHE}$	exergy of air leaving the EAHE system (kWh)
$\dot{X}_{th}$	thermal exergy gained from the BIPVT-EAHE system (kWh)
$\dot{X}_{th,BIPVT}$	thermal exergy gained from the BIPVT system (kWh)
$\dot{X}_{th,EAHE}$	thermal exergy gained from the EAHE system (kWh)

Greek symbols

α_{pv}	absorptance of PV modules
μ	air viscosity (kg m^{-1} s^{-1})
δ_{ins}	thickness of insulation material (m)
ε	effectiveness of EAHE system
ε_b	emissivity of back wall
ε_{pv}	emissivity of PV module
η_{el}	electrical conversion efficiency of PV modules
η_{fan}	fan efficiency

ρ	air density (kg m^{-3})
σ	Stefan-Boltzmann constant (5.67×10^{-8} W m^{-2} K^{-4})

1. Introduction

According to the International Energy Agency (IEA), 36% of the global final energy consumption is accounted by buildings and buildings construction sector which are also responsible for 40% of total direct and indirect CO_2 emissions (IEA, 2019). In the buildings, the rate of increase in global energy usage and CO_2 emission are both 1% each year (IEA, 2019). Buildings also account for more than 55% of the global electricity demand which increases with the yearly rate of 2.5% (IEA, 2019). To decrease the huge amount of direct and indirect CO_2 emissions, the use of renewable energies have been recommended (Chu et al., 2016).

Photovoltaic (PV) systems have been widely used for generating electricity in the world. The amount of electricity produced by PV modules accounts for 2.1% of the global electricity demand equals to 401 GW which increases by 34% growth year-on-year of new installations (Chu et al., 2016). In buildings, the PV modules can be used directly for electricity generation to provide a part of the required electricity. However, the efficiency of the modules reduces by boosting their temperature (Prapas et al., 1987; Brogren et al., 2001; Wu et al., 2017). A possible attractive option which results in the simultaneous production of electricity and heat as well as the enhancement of the PV efficiency is the employment of PVT systems (Norton et al., 2011). In the PVT collectors, a PV module and a heat exchanger are combined as an integrated system which provides a sustainable solution for the built environment (Benemann et al., 2001; Tiwari et al., 2018; Tiwari et al., 2018). The heat exchanger is responsible to gain heat from the PV module to reduce its temperature. The gained thermal energy can also be utilized for heating/cooling purposes in buildings which shows a great potential in HVAC systems (Al-Waeli et al., 2017). Chow et al. (2003) examined a large scale BIPVT system in a subtropical hotel in China. They simulated the performance of the system using ESP-r building energy simulation software and showed the improved electrical efficiency of the system. Furthermore, they utilized the gained heat to decrease the heating load of building. Chow et al. (2009) studied the energy matrices of a water-cooled BIPVT collector for Hong Kong climatic conditions. After presenting the advantages of the proposed system, they reported the yearly thermal and PV module efficiencies of 37.5% and 9.39%, respectively. Shahsavar et al. (2013, 2018) proposed a novel BIPVT collector to provide a part of the heating load of a building as well as cool the PV modules. The gained heat from the PV modules was then used to preheat the outdoor air. They reported that the annual electrical and thermal energy savings potential of the system is respectively 178.2 kWh and 3400.4 kWh. Agathokleous et al. (2018) evaluated the energetic and exergetic performances of a naturally ventilated BIPVT collector. They showed the energy and exergy efficiencies of the system are in the range of 26.5-33.5% and 13-16%, respectively.

Geothermal energy is attractive as an energy source mainly because of its enormous potential and ability to provide base-load power (Lund and Boyd, 2016). In contrast to wind and solar energies that are dependent on the weather conditions and time of day and year, the geothermal system is not restricted to specific countries and can provide energy anywhere in the world. The earth's constant temperature makes geothermal systems as one of the most efficient for heating/cooling purpose (Barbier, 1997). For air heating and cooling, geothermal energy can be used directly by forwarding the cold/warm air to the earth in winter/summer to provide warm/cold air for heating/cooling purposes. It can also be used by a second heat transfer fluid in a heat exchanger indirectly. Due to the significant advantages of the geothermal energy, several researchers have been attracted to use the earth as a heat source to provide all or a part of the heating/cooling load. Bojic et al. (1997) numerically studied an

EAHE integrated with a building using 100% fresh air for heating/cooling purposes and proved that the system could provide a noticeable part of the heating/cooling load of the building. Al-Ajmi et al. (2006) developed a theoretical model to forecast the outlet temperature of an EAHE for cooling purposes in a hot, arid climate. The building simulation was also performed using TRNSYS software and showed a 30% reduction of the cooling energy demand over the peak summer season. The EAHE showed a cooling load reduction of 1700 W with an indoor temperature reduction of 2.8 °C. Jakhar et al. (2016) simulated an earth-water heat exchanger (EWHE) for India using TRNSYS software. They performed a parameter study and compared the findings with an existed concentrating PV (CPV) system. The better performance of the proposed EWHE system was reported as compared with the CPV system using a pipe length of 60 m in the depth of 3.5 m for pipe burial.

Recently, hybrid renewable systems have attracted significant attention due to the simultaneous use of different renewable energies. The hybrid usage of PVT integrated with EAHE to provide required electricity and heating/cooling load of a building is rarely discussed in the literature (Nayak and Tiwari, 2010; Jakhar et al., 2018; Mahdavi et al., 2019). Nayak and Tiwari (2010) studied the performance of an integrated PVT-EAHE system for a greenhouse for various climatic conditions of India. In their system, both the PVT and EAHE systems were used to preheat the air entering the greenhouse. The outcomes showed that Jodhpur is the best place due to greater solar intensity. Jakhar et al. (2018) numerically assessed the thermal performance of a PVT-EAHE system for climatic conditions of Pilani, Ajmer (India) and Las Vegas (USA). The system was able to preheat the cold ambient air by passing it through the PVT and EAHE systems and generate electricity. The heating capacity of the EAHE was observed to be augmented with PVT system by 0.024 kWh to 0.299 kWh, 0.071 kWh to 0.316 kWh and 0.041 kWh to 0.271 kWh for the Pilani, Ajmer and Las Vegas, respectively. Mahdavi et al. (2019) theoretically evaluated the energetic and exergetic performances of a PVT-EAHE system integrated into a solar greenhouse. In the proposed system, the greenhouse air was preheated/precooled by passing through the EAHE system and returned back to the greenhouse. Air inside the greenhouse was also preheated by passing it through the channel located under the PV panels. The results revealed that the PVT system was not able to considerably preheat the greenhouse air. However, the hybrid PVT-EAHE seemed promising in preheating/precooling the greenhouse air by 9 °C and 8 °C in summer/winter, respectively.

The aim of this paper is to analyse the performance of two novel configurations of the BIPVT-EAHE system for climatic conditions of Kermanshah, Iran. Both configurations are able to preheat/precool the outdoor air and generate electricity. In addition, these innovative configurations utilize the building exhaust air to cool the PV panels during the warm months. To the best of our knowledge, the use of exhaust air in the hybrid PVT-EAHE systems has not yet been evaluated in any study. The energy and exergy analysis of the proposed configurations of the BIPVT-EAHE system are performed comprehensively. Then, the effects of different influential parameters on the energetic and exergetic aspects of the best configuration of the BIPVT-EAHE system are examined. The system is evaluated for Kermanshah city in the west of Iran (34.33°N, 47.08°E) with relatively high annual solar radiation of about 7045 MJ/m^2 based on the Iranian Meteorological Organization (IMO) (Khaki et al., 2017).

2. System description

Figs. 1 and 2 display the schematic sketch of the suggested configurations of the BIPVT-EAHE system. Both configurations have two modes of heating and cooling. For the first configuration (configuration A), in the heating mode, the cold outdoor air enters the EAHE system where it is preheated by receiving the heat from the surrounding soil. Then, this preheated air enters the BIPVT collector and is preheated again by absorbing the surplus thermal energy of the PV modules. This results in the cooling of PV modules and consequently, their electrical efficiency augments. In the cooling mode of the first configuration, the hot outdoor air is precooled by transferring heat to the surrounding soil. Besides, the building exhaust air is passed through the duct located underneath the PV modules and thereby reduces their temperature and increases their efficiency. As Fig. 2 shows, for the second configuration (configuration B), in the heating mode, the outdoor air enters the BIPVT collector and then passes through the EAHE system. This causes the air passing through the BIPVT collector to be cooler in the second configuration than in the first configuration and, therefore, the modules are better cooled in the second configuration. Conversely, the temperature difference between the air entering the EAHE system and soil temperature is less in the second configuration than in the first; which leads to lower efficiency of the EAHE system in the second configuration. Additionally, it is seen that the cooling mode of operation is the same for both configurations. It should be noted that both configurations generates electricity, part of which consumes by fans to circulate air through the BIPV/T and EAHE systems, and the rest can cover part of the electricity demand of the building.

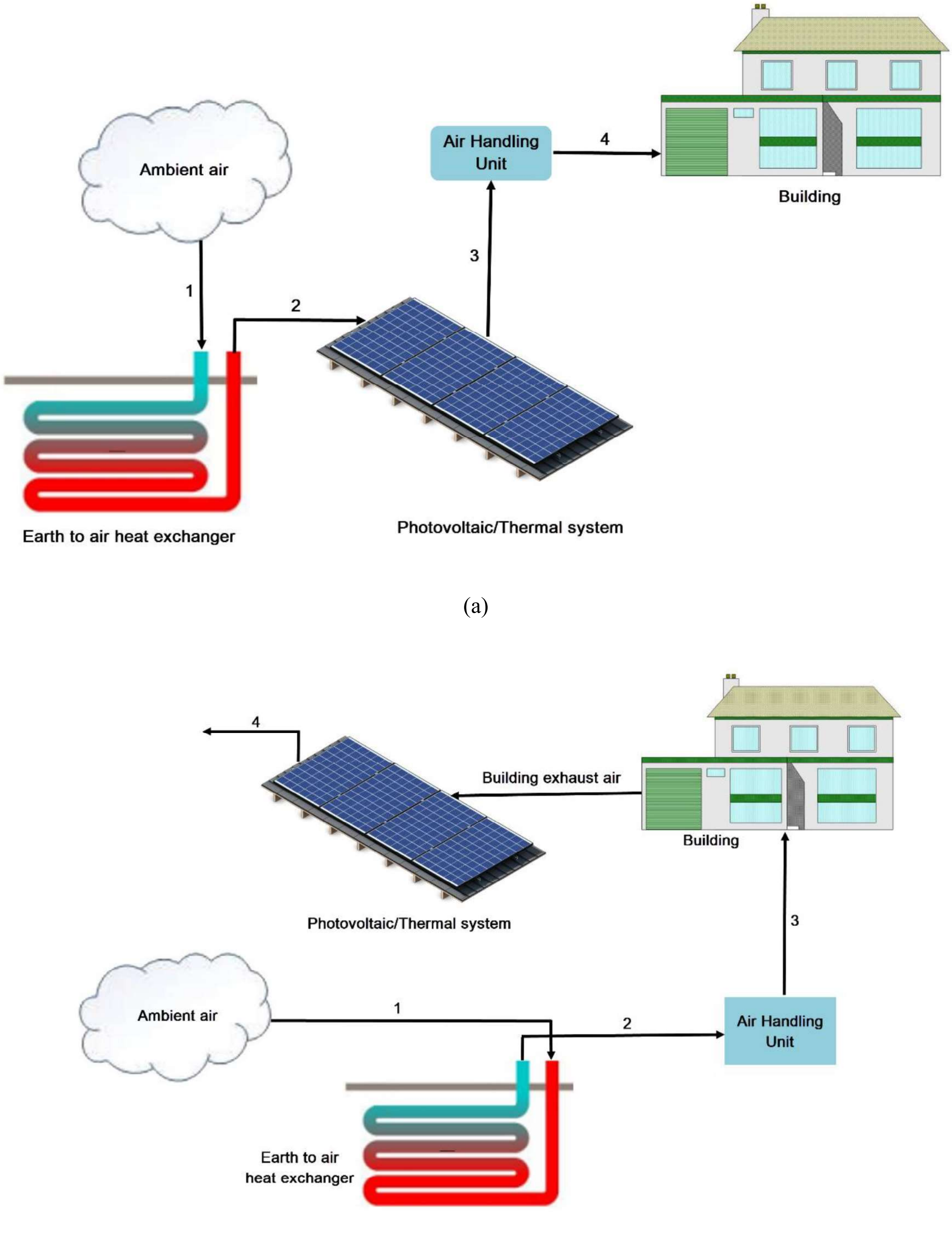

Fig. 1. The working concept of the configuration A: (a) heating mode and (b) cooling mode.

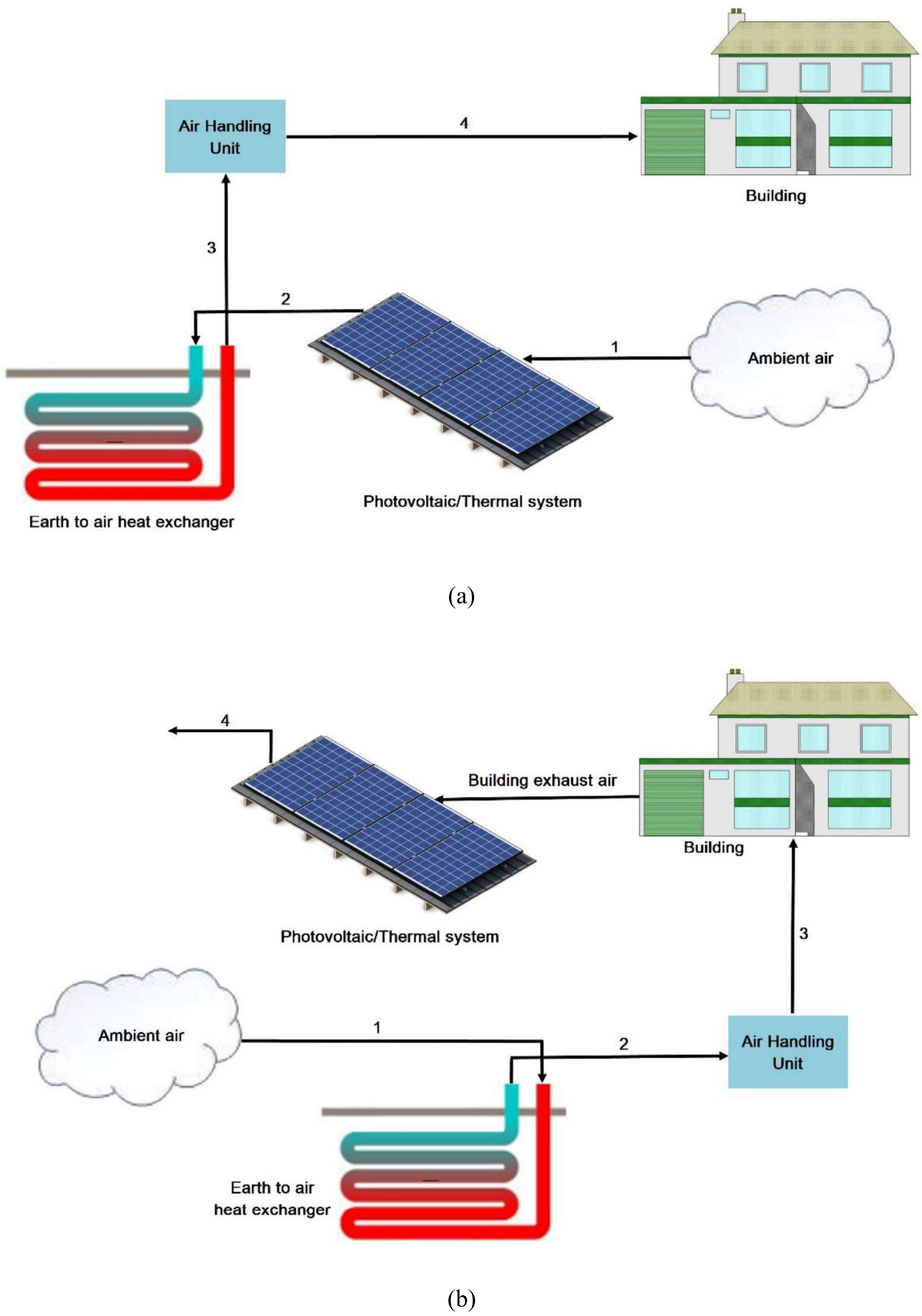

Fig. 2. The working concept of the configuration B: (a) heating mode and (b) cooling mode.

3. Mathematical Modelling

3.1. BIPVT collector

The energy balance equations for different layers of the PVT collector are written under the following assumptions (Khaki et al., 2017):

(1) Heat transfer is one-dimensional steady-state.

(2) Convection heat transfer coefficient is constant over the entire duct.

(3) Temperature is uniform over the PV module and back insulation surface.

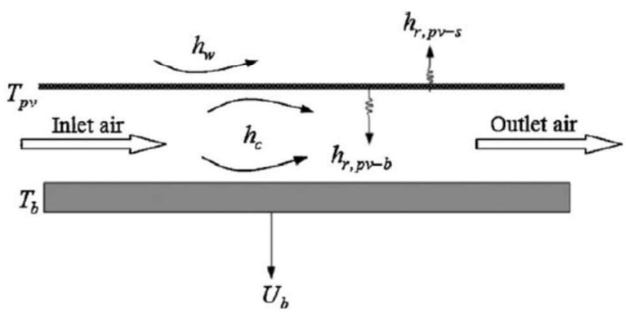

Fig. 3. The Schematic view of the suggested PVT collector.

Therefore, the energy balance equations are as follows (Shahsavar and Rajabi, 2018; Khaki et al., 2017):

For PV modules:

$$\alpha_{pv}(1-\eta_{el})I_r W dx = \left(h_{r,pv-s}+h_w\right)\left(T_{pv}-T_a\right)W dx + h_c\left(T_{pv}-T_f\right)W dx + h_{r,pv-b}\left(T_{pv}-T_b\right)W dx \tag{1}$$

For air stream:

$$\dot{m}_f c_p dT_f = h_c\left(T_{pv}-T_f\right)W dx + h_c(T_b - T_f)W dx \tag{2}$$

For back insulation surface:

$$h_{r,pv-b}\left(T_{pv}-T_b\right)W dx = U_b(T_b - T_a)W dx + h_c\left(T_b - T_f\right)W dx \tag{3}$$

From Eqs. (1) and (3), Eq. (2) can be written as follows:

$$\frac{dT_f}{dx} + A_1 T_f = A_2 \tag{4}$$

where

$$\mathrm{A}_1 = \frac{h_c W}{\dot{m}_f c_p}\,(2 - \mathrm{A}_{1-1} - \mathrm{A}_{1-2}) \tag{5a}$$

$$\mathrm{A}_{1-1} = \frac{(h_c + (\,h_{r,pv-b} h_c / h_{r,pv-b} + U_b + h_c))/\,h_w + h_{r,pv-s} + h_c + h_{r,pv-b}}{1 - (h_{r,pv-b}^2\,/\,(h_w + h_{r,pv-s} + h_c + h_{r,pv-b})(h_{r,pv-b} + U_b + h_c))} \tag{5b}$$

$$\mathrm{A}_{1-2} = \frac{\dfrac{h_{r,pv-b}((h_c + (\,h_{r,pv-b} h_c/(h_{r,pv-b} + U_b + h_c)))/\,(h_w + h_{r,pv-s} + h_c + h_{r,pv-b}))}{1 - (h_{r,pv-b}^2\,/\,(h_w + h_{r,pv-s} + h_c + h_{r,pv-b})(h_{r,pv-b} + U_b + h_c))} + h_c}{h_{r,pv-b} + U_b + h_c} \tag{5c}$$

and

$$\mathrm{A}_2 = \frac{h_c W}{\dot{m}_f c_p}\,(\mathrm{A}_{2-1} + \mathrm{A}_{2-2}) \tag{6a}$$

$$A_{2-1} = \frac{\alpha_{pv}(1 - \eta_{el})I_r + \left(\,h_w + h_{r,pv-s}\right)T_a + \dfrac{\left(\dfrac{h_{r,pv-b} U_b T_a}{h_{r,pv-b} + U_b + h_c}\right)}{h_w + h_{r,pv-s} + h_c + h_{r,pv-b}}}{1 - (h_{r,pv-b}^2\,/\,(h_w + h_{r,pv-s} + h_c + h_{r,pv-b})(h_{r,pv-b} + U_b + h_c))} \tag{6b}$$

$$A_{2-2} = \frac{\dfrac{h_{r,pv-b}\dfrac{\alpha_{pv}(1 - \eta_{el})I_r + \left(\,h_w + h_{r,pv-s}\right)T_a + \dfrac{h_{r,pv-b} U_b T_a}{h_{r,pv-b} + U_b + h_c}}{h_w + h_{r,pv-s} + h_c + h_{r,pv-b}}}{1 - ({h^2}_{r,pv-b}\,/\,(h_w + h_{r,pv-s} + h_c + h_{r,pv-b})(h_{r,pv-b} + U_b + h_c))} + U_b T_a}{h_{r,pv-b} + U_b + h_c} \tag{6c}$$

By using boundary condition (i.e. $T_f\big|_{x=0} = T_{in,BIPV/T}$), T_f is obtained as:

$$T_f(x) = \left(\,T_{in,BIPV/T} - \frac{A_2}{A_1}\right) e^{-A_1 x} + \frac{A_2}{A_1} \tag{7}$$

which results in the outlet air temperature of:

$$T_f(L) = \left(\,T_{in,BIPV/T} - \frac{A_2}{A_1}\right) e^{-A_1 L} + \frac{A_2}{A_1} \tag{8}$$

The average air temperature is given as:

$$T_{mf} = \frac{1}{L}\int_{0}^{L} T_f(x)\,dx = \left(T_{in,BIPV/T} - \frac{A_2}{A_1}\right)\frac{1}{A_1}\left(1 - e^{-A_1 L}\right) + \frac{A_2}{A_1}L \tag{9}$$

By using the average air temperature, the PV modules and back insulation temperatures are calculated as:

$$T_{pv} = A_{2-1} + A_{1-1}T_{mf} \tag{10}$$

$$T_b = A_{2-2} + A_{1-2}T_{mf} \tag{11}$$

The wind-induced exterior heat exchange coefficient is computed as (Duffie and Beckman, 2013):

$$h_w = 2.8 + 3v_w, \quad v_w < 7\ \text{m/s} \tag{12}$$

where v_w is the wind velocity.

The convective heat transfer coefficient of air inside the duct is obtained as (Tan and Charters, 1969):

$$h_c = \frac{k}{D_{H,BIPVT}}\left\{0.0182{Re_{BIPVT}}^{0.8}Pr^{0.4}\left[1 + j\frac{D_{H,BIPVT}}{L}\right]\right\} \tag{13}$$

$$\begin{aligned} j &= 14.3\log\left(\frac{L}{D_{H,BIPVT}}\right) - 7.9 \quad \text{for} \quad 0 < \frac{L}{D_{H,BIPVT}} \le 60 \\ &= 17.5 \quad \text{for} \quad \frac{L}{D_{H,BIPVT}} > 60 \end{aligned} \tag{14}$$

where k is the thermal conductivity of air and $D_{H,PV/T}$ is the hydraulic diameter of the duct below the PV modules ($= 2WS/(W + S)$).

The radiative heat exchange coefficient between the PV modules and sky is calculated as (Khaki et al., 2017; Duffie and Beckman, 2013):

$$h_{r,pv-s} = \sigma\varepsilon_{pv}\frac{\left(T_{pv}^4 - T_s^4\right)}{T_{pv} - T_a} \tag{15}$$

where T_s is the equivalent sky temperature given as (Duffie and Beckman, 2013):

$$T_s = 0.0552T_a^4 \tag{16}$$

The radiative heat exchange coefficient between the PV modules and back wall is calculated as (Duffie and Beckman, 2013):

$$h_{r,pv-b} = \sigma(T_{pv} + T_b)(T_{pv}^2 + T_b^2)\left(\frac{1}{\varepsilon_{pv}} + \frac{1}{\varepsilon_b} - 1\right) \tag{17}$$

For the conduction losses through the back insulation layer, the bottom heat loss coefficient is given as (Khaki et al., 2017):

$$U_b = \frac{k_{ins}}{\delta_{ins}} \tag{18}$$

where k_{ins} is the thermal conductivity of the insulation material and δ_{ins} is the thickness of the insulation material.

3.2. EAHE system

In the earth-air heat exchanger, the heat is transferred to/from the air flows through the pipe walls in the earth by convection and from pipe walls to the surrounding soil and vice versa by conduction. Effectiveness-number of transfer units ($\varepsilon - \mathrm{NTU}$) method is used to evaluate the heat transfer performance of the EAHE system defined as the ratio of the actual heat transfer to the maximum possible heat transfer (Bisoniya, 2015):

$$\varepsilon = \frac{\dot{Q}_{EAHE}}{\dot{Q}_{EAHE,max}} = \frac{T_{out,EAHE} - T_{in,EAHE}}{T_{soil} - T_{in,EAHE}} \tag{19}$$

where $T_{in,EAHE}$ is the inlet air temperature, $T_{out,EAHE}$ is the outlet air temperature of , and T_{soil} is the soil temperature. The temperature of earth at a depth of 1.5 to 2 m remains fairly constant throughout the year called earth's undisturbed temperature (EUT) (De Paepe and Janssens, 2003). The EUT temperature is defined as the yearly mean outdoor air temperature of a specific location which is equals to 295.3 K for Kermanshah, Iran (Khaki et al., 2017).

The effectiveness is also calculated as (Bisoniya, 2015):

$$\varepsilon = 1 - exp(-\mathrm{NTU}) \tag{20}$$

where NTU is the number of transfer units given as (Bisoniya, 2015):

N (21)

and A is the surface area of heat transfer given as:

$$A = \pi D_{i,EAHE} L_{EAHE} \quad (22)$$

Here, $D_{i,EAHE}$ and L_{EAHE} respectively denote the inner diameter and length of EAHE system. In Eq. (21), h is the convective heat exchange coefficient determined as (De Paepe and Janssens, 2003):

$$h = 3.66\frac{k}{D_{i,EAHE}} \qquad \text{if } Re_{EAHE} < 2300 \quad (23a)$$

$$h = \frac{k}{D_{i,EAHE}}\left[\frac{(\xi/8)(Re_{EAHE} - 1000)Pr}{1 + 12.7\sqrt{\xi/8}(Pr^{2/3} - 1)}\right] \qquad if\ 2300 \leq Re_{EAHE} < 5 \times 10^6 \quad (23a)$$

where

$$\xi = (1.82\log Re_{EAHE} - 1.64)^{-2} \qquad \text{if } Re_{EAHE} > 2300 \quad (24)$$

The effectiveness is computed by applying Eqs. (20)-(24) which is then used to calculate the outlet air temperature as:

$$T_{out,EAHE} = T_{in,EAHE} + \varepsilon(T_{soil} - T_{in,EAHE}) \quad (25)$$

3.3. Performance evaluation

For the fresh air, the rate of thermal energy received from the system is obtained as:

$$\dot{Q} = \dot{Q}_{BIPV/T} + \dot{Q}_{EAHE} \quad (26)$$

where

$$\dot{Q}_{BIPV/T} = \dot{m}_f c_p\left[T_f(L) - T_{in}\right] \quad (27)$$

$$\dot{Q}_{EAHE} = \dot{m}_f c_p(T_{out,EAHE} - T_{in,EAHE}) \quad (28)$$

The rate of produced electricity by the BIPVT-EAHE system is given as:

$$\dot{E} = \dot{E}_{BIPV/T,net} - \dot{E}_{EAHE} \tag{29}$$

316 where

$$\dot{E}_{BIPVT,net} = \alpha_{pv}\eta_{el}I_r WL - \dot{E}_{fan,BIPVT} \tag{30}$$

$$\eta_{el} = 0.125\left[\,1 - 0.006\left(T_{pv} - 298\right)\right] \tag{31}$$

317 where $\dot{E}_{fan,BIPVT}$ and $\dot{E}_{EAHE}$ are respectively the fan consumed power to blow air inside the
318 BIPVT and EAHE systems, which are obtained using the following equation (Khaki et al.,
319 2017):

$$\dot{E}_{fan} = \frac{(\dot{m}_f/\rho)\Delta P}{\eta_{fan}} \tag{32}$$

320 η_{fan} is the fan efficiency. Furthermore, ΔP is the pressure loss through the duct given as
321 (Khanmohammadi and Shahsavar, 2018):

$$\Delta P_{BIPVT} = \frac{1}{2}k_{c,BIPVT}\frac{\dot{m}_f^2}{\rho(WS)^2} + f_{BIPVT}\frac{L}{D_{H,BIPVT}}\frac{\dot{m}_f^2}{\rho(WS)^2} \tag{33}$$

$$\Delta P_{EAHE} = \frac{1}{2}k_{c,EAHE}\frac{\dot{m}_f^2}{\rho\left(\frac{\pi}{4}D_{i,EAHE}^2\right)^2} + f_{EAHE}\frac{L_{EAHE}}{D_{i,EAHE}}\frac{\dot{m}_f^2}{\rho\left(\frac{\pi}{4}D_{i,EAHE}^2\right)^2} \tag{34}$$

322 where $k_{c,BIPVT}$ and $k_{c,EAHE}$ are the inlet and outlet loss coefficients for the BIPVT and EAHE
323 systems, respectively. Moreover, f_{BIPVT} and f_{EAHE} are respectively the fanning friction
324 factors for the BIPVT and EAHE systems, computed as (Jakhar et al., 2017):

$$f_{BIPVT} = \frac{0.079}{{Re_{BIPVT}}^{0.25}} \tag{36}$$

$$f_{EAHE} = \frac{0.079}{{Re_{EAHE}}^{0.25}} \tag{37}$$

325 where Re_{BIPVT} and Re_{EAHE} are the Reynolds number of air inside the BIPVT collector and
326 EAHE, respectively, estimated as:

$$Re_{BIPVT} = \frac{\dot{m}_f D_{H,BIPVT}}{WS\mu} \tag{38}$$

$$Re_{EAHE} = \frac{4\dot{m}_f}{\pi D_{i,EAHE}\mu} \tag{39}$$

To examine the overall energetic aspect of the BIPVT-EAHE system, a new parameter called the Energetic Performance Evaluation Criterion ($\mathrm{PEC_{en}}$) is defined as the ratio of the total thermal and electrical power received from the system to the heating/cooling load of the outdoor air, given as:

$$\mathrm{PEC_{en}} = \frac{\dot{Q} + \left(\dot{E}/0.36\right)}{\dot{m}_f c_p |296 - T_a|} \tag{40}$$

where the coefficient 0.36 is the conversion factor of the thermal power plant (Shahsavar et al., 2018).

3.4. Exergy analysis

According to the Second Law of Thermodynamics, the exergy analysis of the EAHE system is given as:

$$\dot{X}_{in,EAHE} = \dot{X}_{out,EAHE} + \dot{X}_{fan,EAHE} + \dot{X}_{dest,EAHE} \tag{41}$$

In the above equations, $\dot{X}_{in,EAHE}$ is the exergy of inlet air, $\dot{X}_{out,EAHE}$ is the exergy of outlet air, $\dot{X}_{fan,EAHE}$ is the exergy of fun consumed power, and $\dot{X}_{dest,EAHE}$ is the exergy loss from the EAHE system.

The exergy of inlet and outlet air is because of the temperature and is computed as (Khaki et al., 2017):

$$\dot{X}_{in,EAHE} = \dot{m}_f c_p \left[T_{in,EAHE} - T_a - T_a \ln\left(\frac{T_{in,EAHE}}{T_a}\right)\right] \tag{42}$$

$$\dot{X}_{out,EAHE} = \dot{m}_f c_p \left[T_{out,EAHE} - T_a - T_a \ln\left(\frac{T_{out,EAHE}}{T_a}\right)\right] \tag{43}$$

The electrical energy can be completely converted into work and consequently, its exergy amount is equivalent to the energy amount of electrical flow (Khaki et al., 2017). Therefore, the fan consumed exergy is equal to the fan consumed power.

For the BIPVT collector, the exergy analysis is performed as (Khaki et al., 2017):

$$\dot{X}_{in,BIPVT} + \dot{X}_{solar} + \dot{X}_{fan,BIPVT} = \dot{X}_{out,BIPVT} + \dot{X}_{el,PV} + \dot{X}_{dest,BIPVT} \quad (44)$$

where $\dot{X}_{in,BIPVT}$, $\dot{X}_{out,BIPVT}$ and $\dot{X}_{solar}$ are respectively the exergy of inlet air, outlet air and solar light. Moreover, $\dot{X}_{fan,BIPVT}$ and $\dot{X}_{el,PV}$ are the exergy of fan consumed power and electrical exergy of the PV modules, respectively. $\dot{X}_{dest,BIPVT}$ is the exergy loss from the BIPVT system.

The exergy of inlet and outlet air streams are calculated as (Khaki et al., 2017):

$$\dot{X}_{in,BIPVT} = \dot{m}_f c_p \left[T_{in,BIPVT} - T_a - T_a \ln\left(\frac{T_{in,BIPVT}}{T_a}\right)\right] \quad (45)$$

$$\dot{X}_{out,BIPVT} = \dot{m}_f c_p \left[T_{out,BIPVT} - T_a - T_a \ln\left(\frac{T_{out,BIPVT}}{T_a}\right)\right] \quad (46)$$

The rate of thermal exergy that the fresh air gains from system is given as:

$$\dot{X}_{th} = \dot{X}_{th,BIPVT} + \dot{X}_{th,EAHE} \quad (47)$$

where

$$\dot{X}_{th,BIPVT} = \dot{m}_f c_p \left[T_{out,BIPVT} - T_{in,BIPVT} - T_a \ln\left(\frac{T_{out,BIPVT}}{T_{in,BIPVT}}\right)\right] \quad (48)$$

$$\dot{X}_{th,EAHE} = \dot{m}_f c_p \left[T_{out,EAHE} - T_{in,EAHE} - T_a \ln\left(\frac{T_{out,EAHE}}{T_{in,EAHE}}\right)\right] \quad (49)$$

The rate of electrical exergy generated by the BIPVT-EAHE system is obtained as:

$$\dot{X}_{el} = \dot{X}_{el,BIPVT} + \dot{X}_{el,EAHE} \quad (50)$$

where

$$\dot{X}_{el,BIPVT} = \alpha_{pv} \eta_{el} I_r W L - \dot{E}_{fan,BIPVT} \quad (51)$$

$$\dot{X}_{el,EAHE} = \dot{E}_{fan,EAHE} \quad (52)$$

Similar to the energy analysis, the overall exergetic performance of the system called as the Exergetic Performance Evaluation Criterion ($\mathrm{PEC_{ex}}$) is defined as the ratio of the total thermal and electrical exergy gained from the system to the exergy load of the fresh air:

$$\mathrm{PEC_{ex}} = \frac{\dot{X}_{th} + \dot{X}_{el}}{\dot{m}_f c_p \left|296 - T_a - T_a \ln\left(\frac{296}{T_a}\right)\right|} \tag{53}$$

4. Results and discussion

In this study, the presented mathematical model has been solved by following an iterative process as depicted in Fig. 4. After the model validation, the energetic and exergetic performances of the two proposed configurations for the BIPVT-EAHE system are examined. For this purpose, firstly, the hourly temperature of outlet air and PV module are presented for a typical cold day (January 15th) and a typical warm day (August 15th). Then, the rates of gained thermal energy and exergy and the net produced electric power are studied in different months for both configurations. Finally, the better system is selected and the variation of effective parameters on the energetic and exergetic performances are analysed. The constant design aspects of the system are presented in Table 1. The solar radiation intensity and outdoor air temperature for a simple day of each month for Kermanshah can be found in Ref. (Shahsavar et al., 2018).

Table 1. Design aspect of the BIPVT-EAHE system under investigation.

c_p, J/kgK	1005	S, m	0.5
$D_{i,EAHE}$, m	0.1	v_w, m/s	1.5
k, W/mK	0.0257	W, m	3
$k_{c,BIPVT}$, W/mK	1.5	α_{pv}	0.9
$k_{c,EAHE}$, W/mK	2.6	δ_{ins}, m	0.025
k_{ins}, W/mK	0.045	ε_{pv}	0.8

L_{EAHE}, m	25	η_{fan}	0.5
L, m	10	μ, kg/ms	0.00001511
$\dot{m}_f$, kg/s	0.01	ρ, kg/m^3	1.2

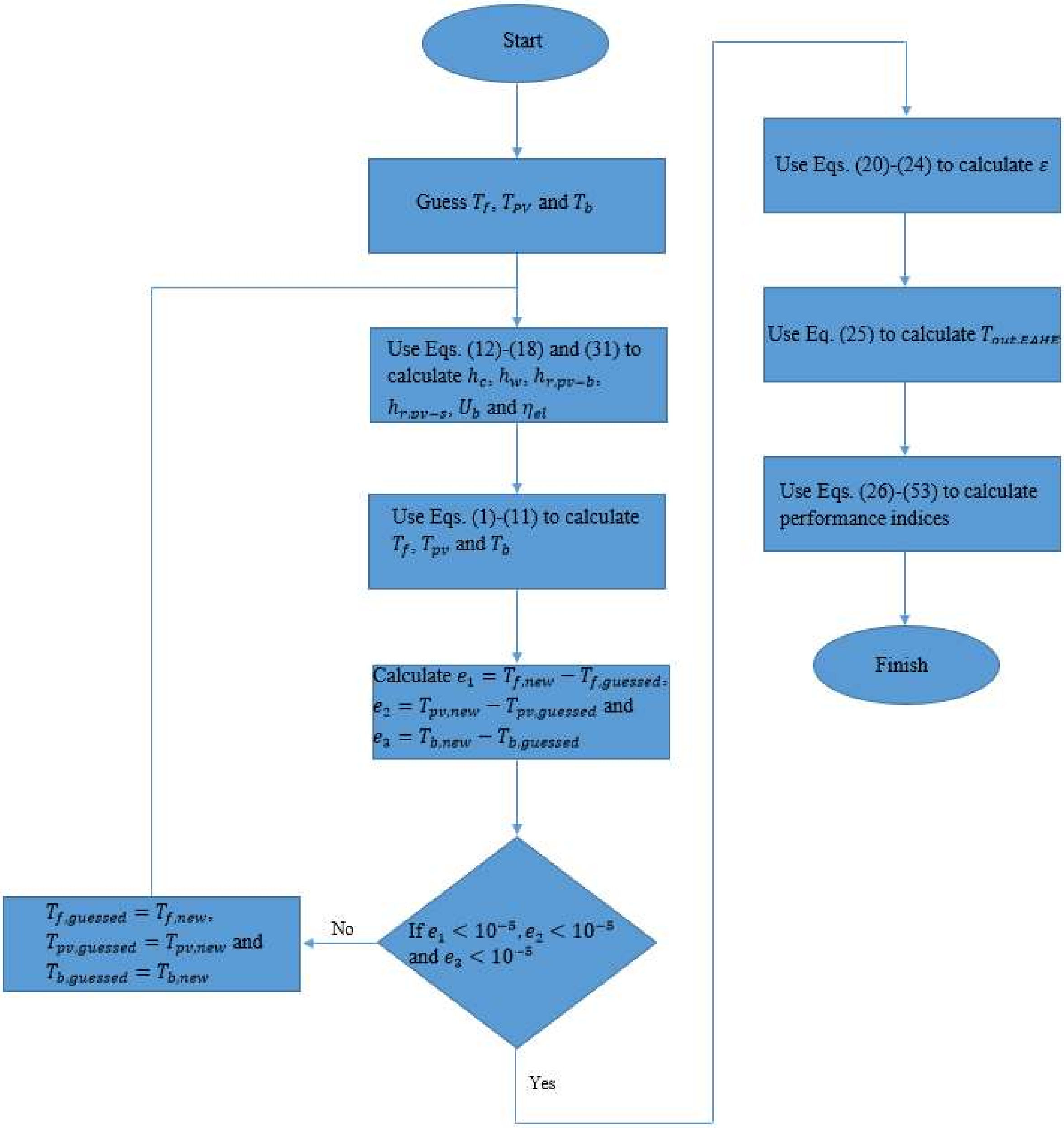

Fig. 4. Flowchart for mathematical modelling of the BIPVT-EAHE system.

4.1. Model validation

The experimental results of Tonui and Tripanagnostopoulos (2007) is employed for comparison based on the PV module temperature and the outlet air temperature. They studied a PVT including a single-pass air duct below the module. Fig. 5 illustrates the comparison of the findings of current investigation with those of Tonui and Tripanagnostopoulos (2007) presenting the accuracy of the present simulation carried out using MATLAB software. Moreover, the PV module temperature and the outlet air temperature obtained in the current study are compared to the experimental findings of Kasaeian et al. (2017) for the case of single-pass air PVT system. This comparison is illustrated in Fig. 6, and it can be observed that there is a suitable consistency between the results.

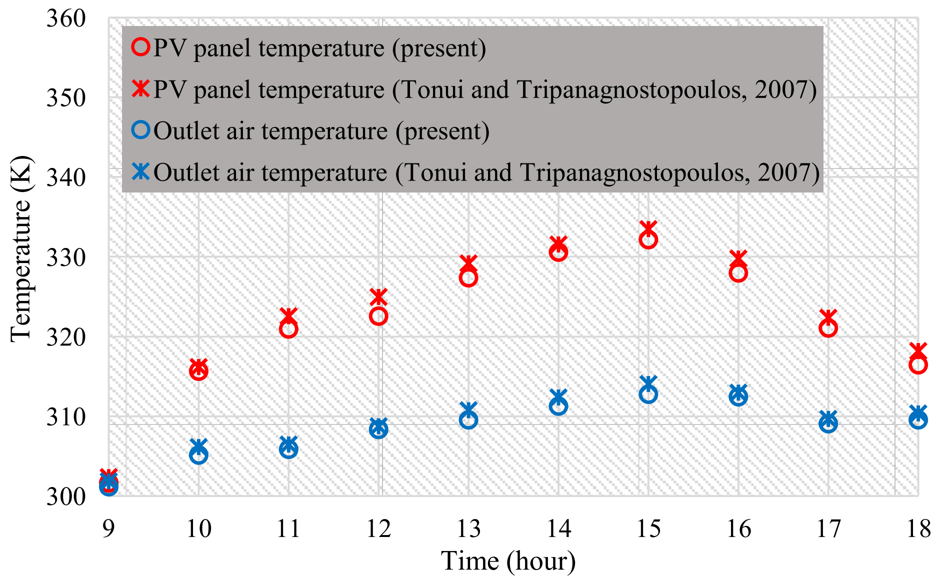

Fig. 5. Comparison between the findings of current assessment with those of Tonui and Tripanagnostopoulos (2007).

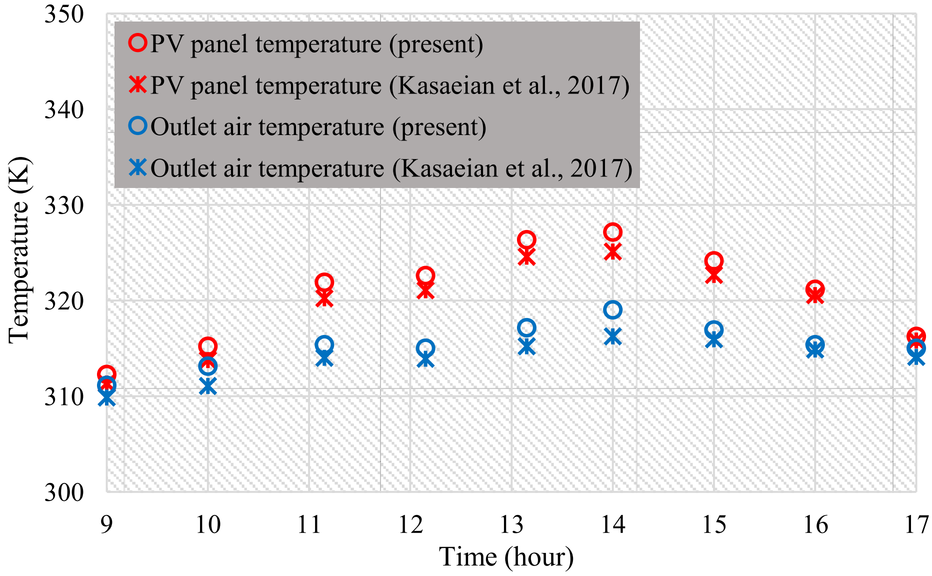

Fig. 6. Comparison between the findings of current assessment with those of Kasaeian et al. (2017).

4.2. Performance analysis

Fig. 7(a) depicts the hourly temperature of preheated air on the 15th of January. The figure also contains the hourly temperature of outdoor air to examine the amount of preheating at each hour. As is seen, the outlet air temperature is the same for both configurations, except from 8 AM to 16 PM. In other hours, the BIPVT collector is inactive, due to the zero radiation intensity, and there is no difference between the performances of different configurations of BIPVT-EAHE system. From 8 AM to 16 PM, the preheated air temperature in the configuration A is 0.47-4.4 °C higher than that of the configuration B and the maximum difference between the results of two configurations occurs at 12 AM. In January, because of the low ambient air temperature and solar radiation intensity, the increase in the temperature of the PV panels is less than the warm months of the year. Therefore, the increase in the air temperature by passing it through the channel located under the PV panels is not high. On the other hand, preheating the ambient air in the BIPVT system and then using it in the EAHE system leads to a reduction in the effectiveness of the EAHE system. These factors reduce the preheating performance of the configuration B compared to the configuration A in which the air first passes through the EAHE system, and then passes through the BIPVT system. Fig. 7(b) illustrates the hourly temperature of precooled air on the August 15th. Both configurations have a similar working principles in the cooling mode and consequently, there is no difference between their precooling results. It can be seen that the suggested system has a great performance in precooling the warm outdoor air. According to the results, the highest precooling of the outdoor air occurs at 3 PM, which is 13.34 °C.

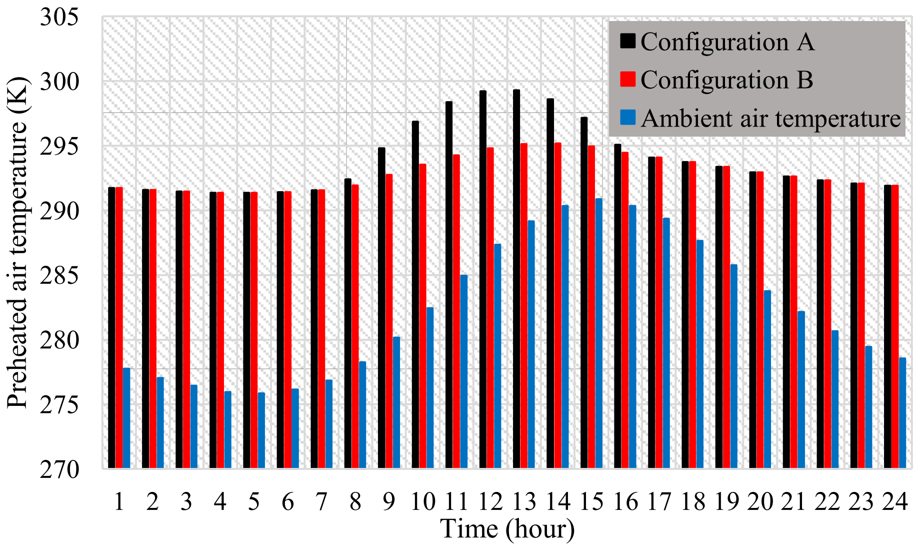

(a)

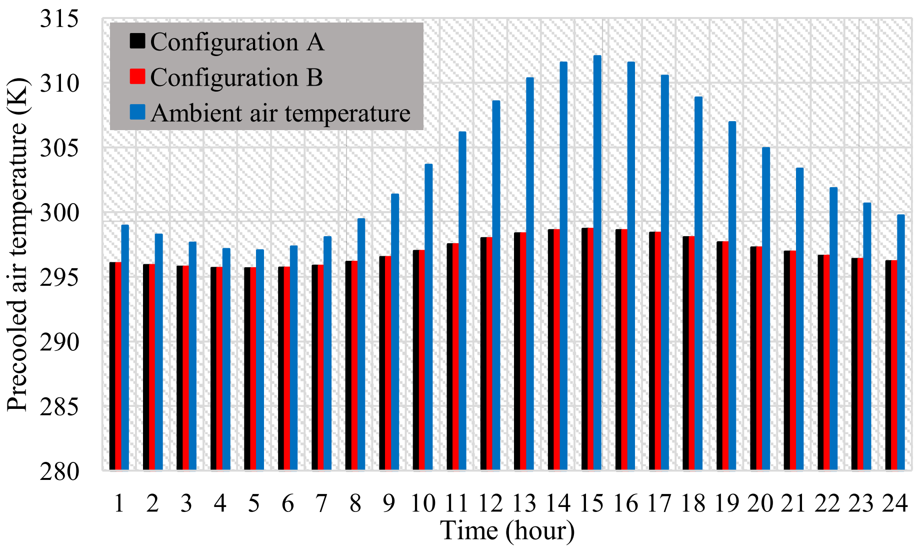

(b)

Fig. 7. Hourly temperature of preheated/precooled air for a (a) sample cold day (15th of January) and (b) sample warm day (15th of August).

The hourly temperature of PV module in two suggested configurations of the BIPVT-EAHE system are depicted in Fig. 8(a) and (b) for the January 15th and August 15th, respectively. It should be noted that the results presented in Fig. 8 are related to the hours at which solar radiation is available. During the studied cold day, the PV panel temperature in the configuration B is 3.63-14.13 °C lower than that of the configuration A, and therefore, the configuration B has a better performance in cooling the PV modules than the configuration A.

In the configuration A, the air passes through the EAHE system before passing under the modules, and gains heat. Thus, the cooling capacity reduces compared to the configuration B. Moreover, Fig. 8(b) shows that the configurations A and B have equal PV module temperatures during the sample warm day, which is because of the similar working principles of the cooling mode of these configurations.

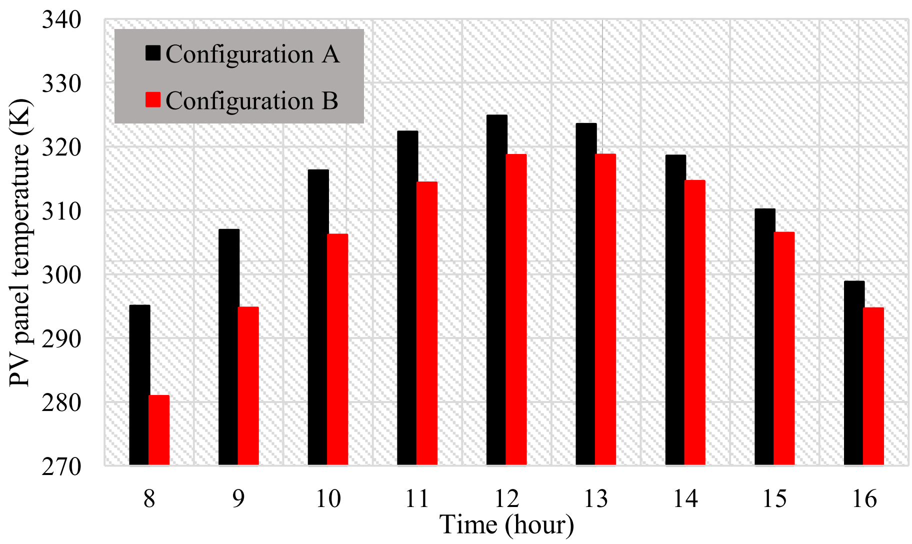

(a)

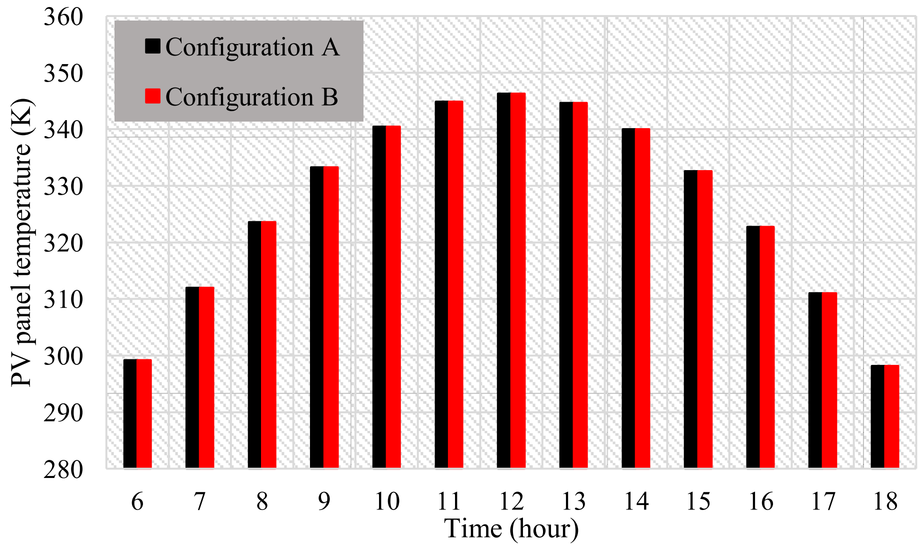

(b)

Fig. 8. Hourly temperature of PV module for a (a) sample cold day (January 15th) and (b) sample warm day (August 15th).

The monthly rate of received thermal energy by air from the two configurations of BIPVT-EAHE system is shown in Fig. 9. In the cooling mode, two configurations have the same performance; however, in the heating mode, except in March and October, the configuration A shows a better performance. During March and October, the ambient air temperature and the solar radiation intensity and, consequently, the PV panel temperature are more than the other cold months of the year. This makes the ambient air pre-heating through the BIPVT system more impressive than the EAHE system. Therefore, during these months, the configuration B represents a better performance than the configuration A, but with a decrease in both the ambient air temperature and solar radiation intensity, the opposite is true and the configuration A performs better than the configuration B. According to the results, the highest rate of thermal energy for both configurations occurs in January (493.62 and 449.63 kWh for configuration A and configuration B, respectively), while the lowest rate of thermal energy belongs to April (160.02 kWh for both configurations). The yearly rate of thermal energy recovered by the configurations A and B are 3499.59 and 3468.16 kWh, respectively.

Hence, it can be said that the configuration A has a slightly better heat transfer performance (0.91%) as compared with the configuration B.

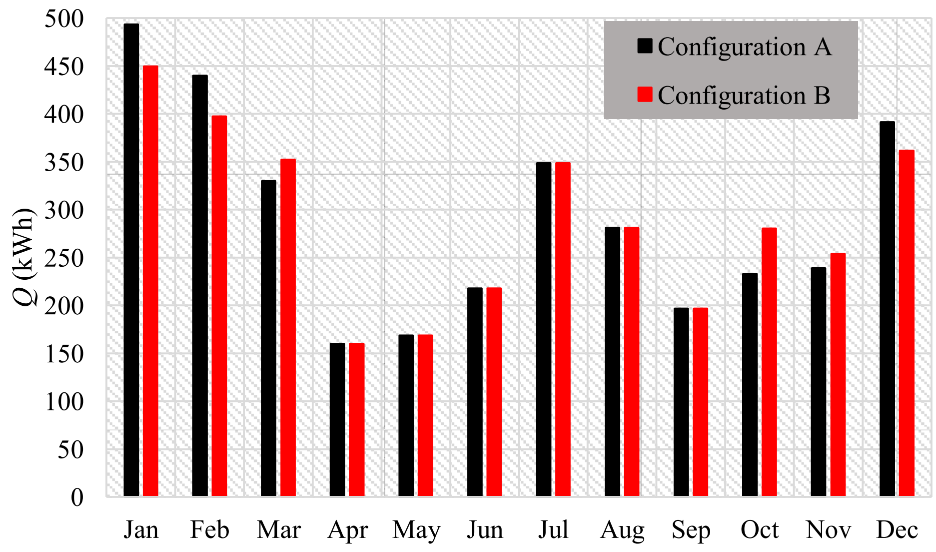

Fig. 9. The monthly thermal power gained from the different configurations of BIPVT-EAHE system

Fig. 10 shows the monthly electric power generated by the suggested configurations of BIPVT-EAHE system. The electricity produced by both configurations are equal in cooling mode; however, in the heating mode, the configuration B presents a better electrical performance compared to the configuration A. This is due to the lower temperature of the PV panels in configuration B in comparison with the configuration A. The maximum difference between the produced electricity in the heating mode of the two configurations occurs in January (4.79%). The yearly total electrical energy produced by the configurations A and B are respectively 5908.19 and 5969.87 kWh. Hence, it can be said that the electrical performance of the configurations B is slightly (1.04%) better than that of the configuration A.

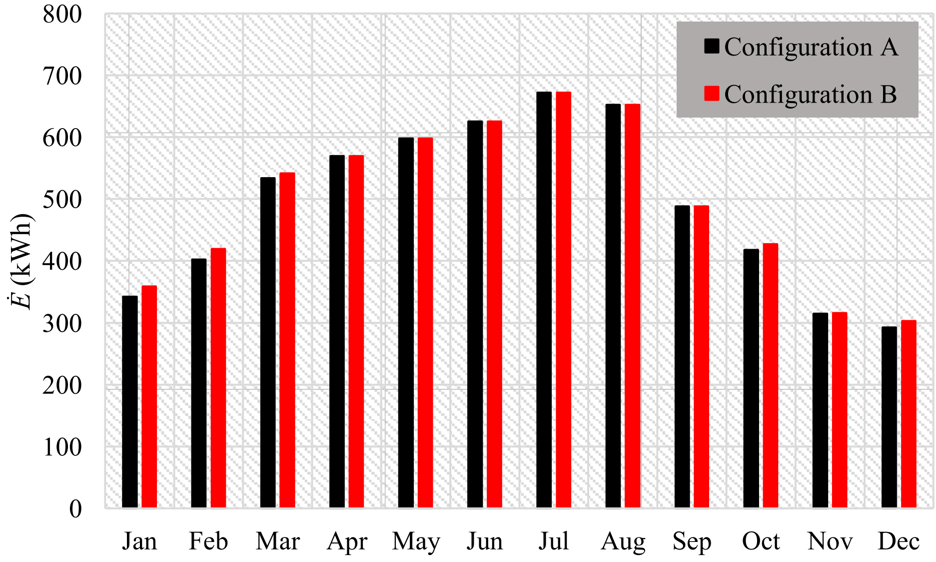

Fig. 10. The monthly electric power generated by the different configurations of BIPVT-EAHE system.

Fig. 11 gives the monthly rate of obtained thermal exergy from the different configurations of BIPVT-EAHE system. As shown, the performance of two configurations is the same in terms of thermal exergy in the cooling mode; however, in cold months, the thermal exergy obtained from the configuration A is better than the configuration B. The maximum difference between the generated rate of thermal exergy by configurations A and B is 19.75%, which occurs in February. The annual total rate of thermal exergy received from configuration A is 55.59 kWh, which is 7.39% higher than that of the configuration B (51.76 kWh).

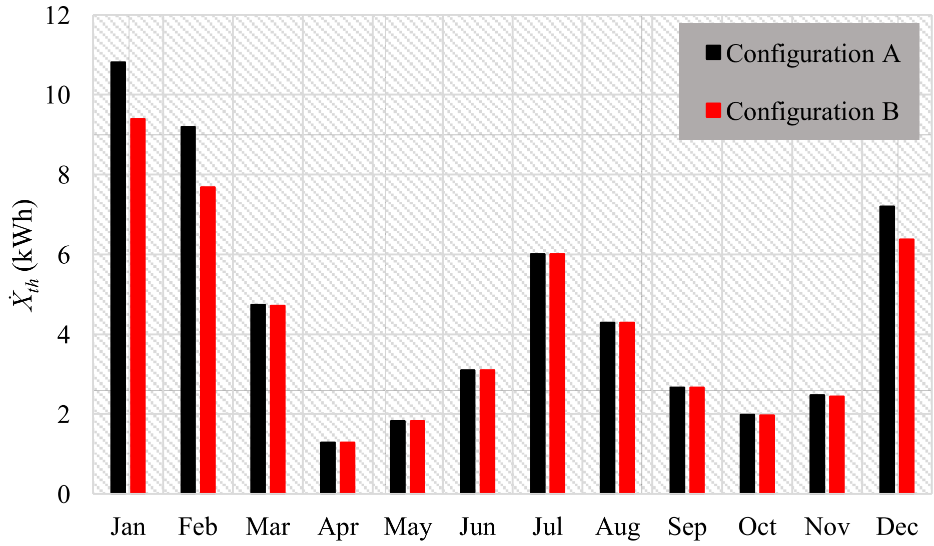

Fig. 11. The monthly rate of thermal exergy produced by the different configurations of BIPVT-EAHE system.

Fig. 12 shows the monthly average PEC_{en} of two configurations of BIPVT-EAHE system. The results show that the energy performance of both configurations are equal in the cooling mode; however, in the heating mode, except in December, the configuration B has a better energy performance than the configuration A. The maximum and minimum values of PEC_{en} of both configurations occurs in May (5.91 for configuration A and 6.05 for Configuration B) and January (2.48 for configuration A and 2.49 for configuration B), respectively. The yearly average PEC_{en} of configurations A and B are respectively 5.81 and 5.85, which indicates that the overall energy performance of configuration B is slightly (0.46%) better than the configuration A. In addition, in Fig. 12, it can be seen that PEC_{en} of both configurations in all months of the year is more than one, which shows that both configurations can provide the required total thermal load of the building.

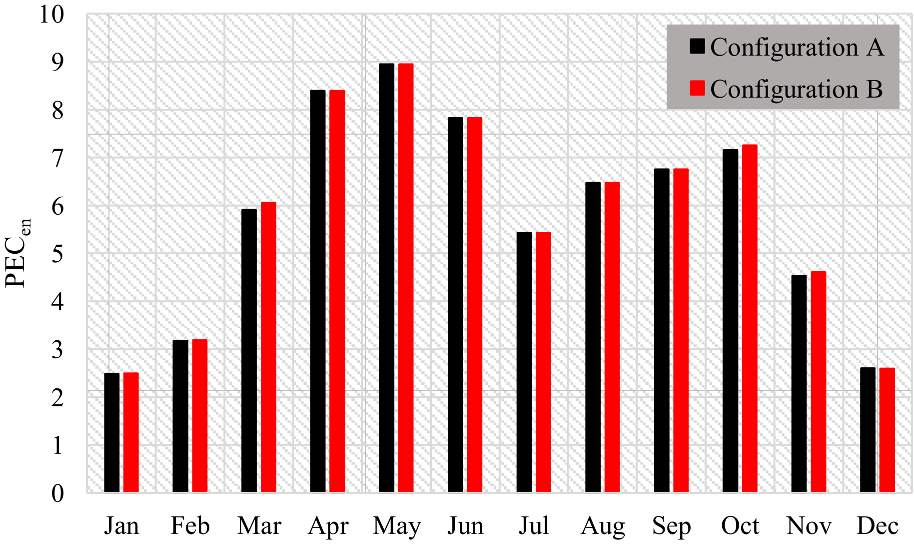

Fig. 12. The monthly average PEC$_{en}$ for different configurations of BIPVT-EAHE system.

The monthly average PEC$_{ex}$ of two configurations of PVT-EAHE system are demonstrated in Fig. 13. The exergy performance of both configurations are equal in the cooling mode; however, in the heating mode, except in October, the configuration B has a better exergy performance than the configuration A. The best exergy performance of both configurations occurs in April, while the worst one occurs in January. The yearly average PEC$_{ex}$ of the configuration A and configuration B is 121.14 and 121.51, respectively, and so it can be said that from the viewpoint of the second law of thermodynamics, the configuration A is slightly (0.02%) better than the configuration B.

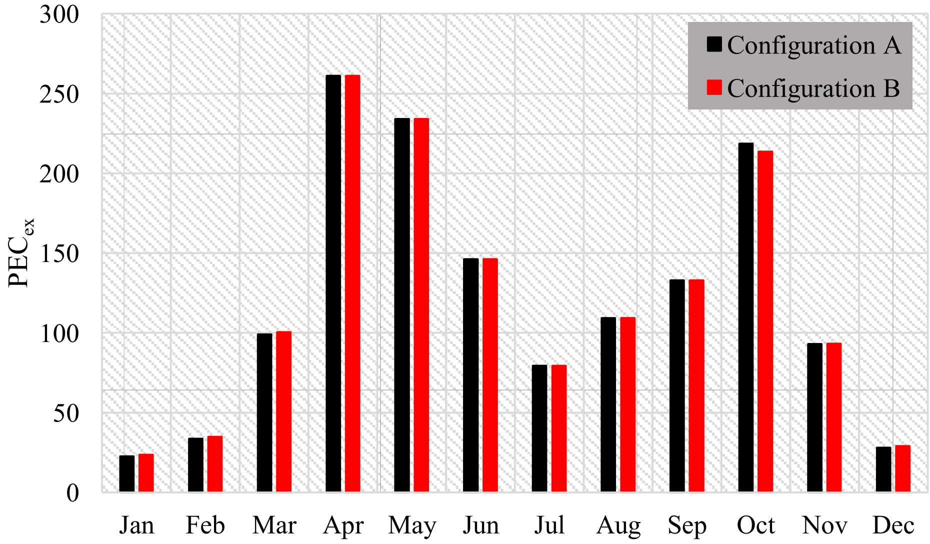

Fig. 13. The monthly average PEC$_{ex}$ for different configurations of BIPVT-EAHE system.

At the end of this section, to better compare the performance of the configurations A and B, the results presented in this section are also tabulated in Table 2.

Table 2. Performance metrics of the different configurations of the BIPVT-EAHE system.

Month	Configuration A					Configuration B				
	$\dot{Q}$ (kWh)	$\dot{E}$ (kWh)	$\dot{Q}$ (kWh)	PEC$_{en}$	PEC$_{ex}$	$\dot{Q}$ (kWh)	$\dot{E}$ (kWh)	$\dot{Q}$ (kWh)	PEC$_{en}$	PEC$_{ex}$
Jan.	493.62	342.20	10.81	2.49	22.62	449.63	358.60	9.40	2.49	23.58
Feb.	439.80	402.30	9.19	3.18	33.62	397.31	419.14	7.68	3.19	34.87
Mar.	329.97	533.97	4.74	5.91	99.10	352.41	541.50	4.72	6.05	100.48
Apr.	160.02	569.45	1.29	8.39	261.23	160.02	569.45	1.29	8.39	261.23
May.	168.61	597.84	1.83	8.95	234.18	168.61	597.84	1.83	8.95	234.18
Jun.	217.78	625.15	3.10	7.83	146.22	217.78	625.15	3.10	7.83	146.22
Jul.	348.67	671.78	6.00	5.43	79.48	348.67	671.78	6.00	5.43	79.48
Aug.	281.20	652.23	4.29	6.48	109.24	281.20	652.23	4.29	6.48	109.24
Sep.	196.70	488.03	2.67	6.76	132.95	196.70	488.03	2.67	6.76	132.95
Oct.	232.94	417.56	1.99	7.15	218.61	280.34	427.38	1.97	7.25	213.60

Nov.	238.78	315.03	2.47	4.54	93.03	253.88	315.90	2.44	4.61	93.28
Dec.	391.49	292.65	7.20	2.60	28.15	361.62	302.87	6.37	2.60	29.03

4.3. Case study

In this section, the impacts of PVT and EAHE parameters on the annual average PEC_{en} and PEC_{ex} of the configuration B are examined. Fig. 14 illustrates the effect of duct length on the annual average PEC_{en} and PEC_{ex} of the configuration B at different duct widths. It is clear that both the annual average PEC_{en} and PEC_{ex} increase by boosting the duct length and duct width. Increasing the duct length results in a higher outlet air temperature and a higher pressure drop, which respectively increases and decreases the annual average PEC_{en} and PEC_{ex}. The results show that the effect of increasing the outlet air temperature is more pronounced, and as a result, the annual average PEC_{en} and PEC_{ex} enhance with intensifying the duct length. The increase in the duct width results in the following consequences:

- Reducing the air velocity which leads to an enhancement in the outlet air temperature and therefore, increases the rate of thermal energy and exergy of the system.
- Reducing the power consumption of fans due to a reduced pressure drop.
- Reducing the produced power of PV modules because of an enhancement in their temperature.
- Increasing the exposure area of the PV modules and consequently, increasing their production capacity.

Generally, the produced power of PV modules enhances with increasing the duct width. Higher values of the annual average PEC_{en} and PEC_{ex} by increasing the duct width shows that the effect of increase in the thermal energy, thermal exergy and produced power of the PV modules outweighs the impact of increase in the fan power consumption.

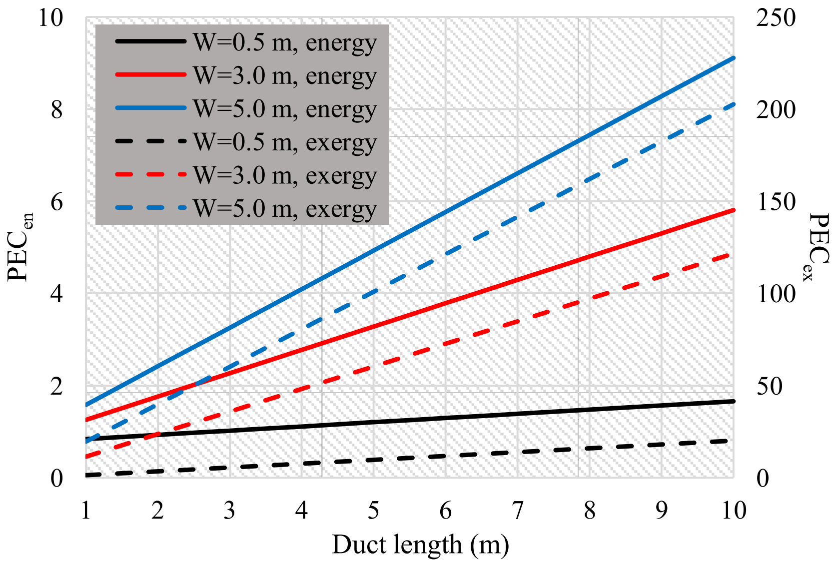

Fig. 14. The variation of yearly average PEC_{en} and PEC_{ex} as a function of duct length for different duct widths for the configuration B of BIPVT-EAHE system.

Fig. 15 gives the impact of air mass flow rate on the annual average PEC_{en} and PEC_{ex} of the configuration B at different duct depths. It is observed that both parameters reduce for a higher air mass flow rate and duct depth. Augmenting the air mass flow rate directly causes an improvement in the rate of obtained thermal energy, according to Eqs. (27) and (28), and thermal exergy, according to Eqs. (48) and (49), from the system. In addition, rising the air mass flow rate reduces the preheated air temperature in the heating mode or increases the precooled air temperature in the cooling mode, resulting in a reduction in the rate of obtained thermal energy and exergy of the system. The findings show that the impact of air mass flow rate on the thermal energy and exergy of the system is greater than the effect of air temperature, and therefore, the rate of thermal energy and exergy gained from the system increases with boosting the air mass flow rate. Moreover, an increase in the air mass flow rate reduces the temperature of the PV modules and, as a result, increases the rate of electricity generated by the modules. In addition, the fan power increases for a higher air mass flow rate, which reduces the annual average PEC_{en} and PEC_{ex} of the system. The results presented in

Fig. 15 show that the impact of boosted fan power outweighs the effects of increased thermal energy, thermal exergy, and generated electricity by the PV modules and therefore, the annual average PEC_{en} and PEC_{ex} decreases with increasing the air mass flow rate. Increasing the duct depth results in a decrease in the air velocity and as a result, both the thermal energy and exergy of the system increase. In addition, increasing the duct depth leads to a reduced rate of electricity produced by the PV modules and the power consumption of fans. Consequently, according to Fig. 15, by increasing the duct depth, the effect of decreasing the produced electricity of the PV modules overcomes the impact of reducing the fan power and therefore, the annual average PEC_{en} and PEC_{ex} of the system augments with boosting the duct depth.

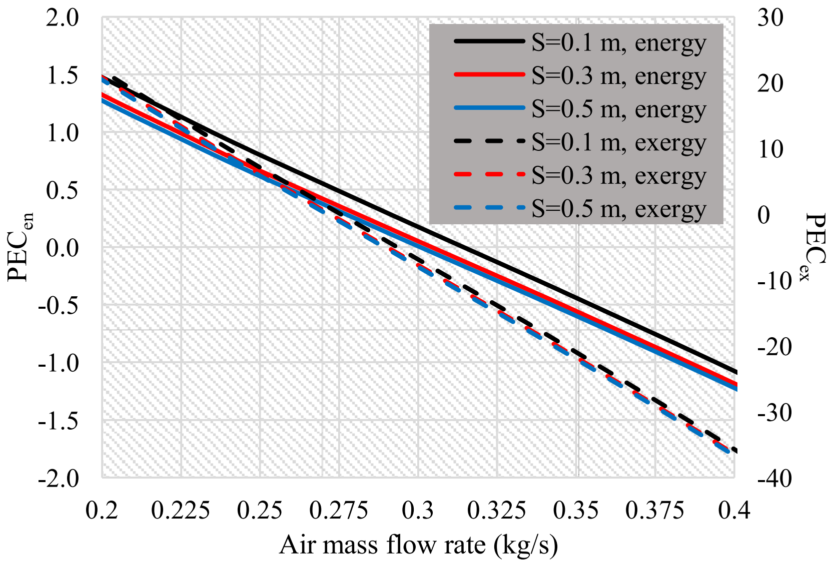

Fig. 15. The variation of yearly average PEC_{en} and PEC_{ex} as a function of air mass flow rate for different duct depths for the configuration B of BIPVT-EAHE system.

Fig. 16 depicts the influence of tube length of EAHE on the annual average PEC_{en} and PEC_{ex} of the configuration B at different tube diameters of EAHE system. The findings show that both the annual average PEC_{en} and PEC_{ex} increase with boosting the tube diameter.

Augmenting the tube diameter results in a higher effectiveness and therefore, higher rate of heat transfer in EAHE system. On the other hand, the air velocity reduces by increasing the tube diameter, which reduces the pressure drop and therefore, the fan power reduces by rising the tube diameter. Hence, the increased annual average PEC_{en} and PEC_{ex} of the configuration B with boosting the tube diameter is due to the increased rate of thermal energy/exergy and reduced fan power. Furthermore, Fig. 16 reveals that intensifying the pipe length in the tube diameters of 0.1 m and 0.5 m leads to a decrease in the annual average PEC_{en}; however, for the inner diameter of 0.3 m, it leads to an increase in the annual average PEC_{en}. Also, the results show that in the tube diameter of 0.1 m, the annual average PEC_{ex} decreases with increasing the tube length, while it is vice versa in the diameters of 0.3 m and 0.5 m. The increase in the pipe length leads to a higher rate of heat transfer in the EAHE system, resulting in a higher annual average PEC_{en} and PEC_{ex}. Besides, the pressure drop and hence, the fan consumed power augment with the increase in pipe length, which results in a lower annual average PEC_{en} and PEC_{ex}.

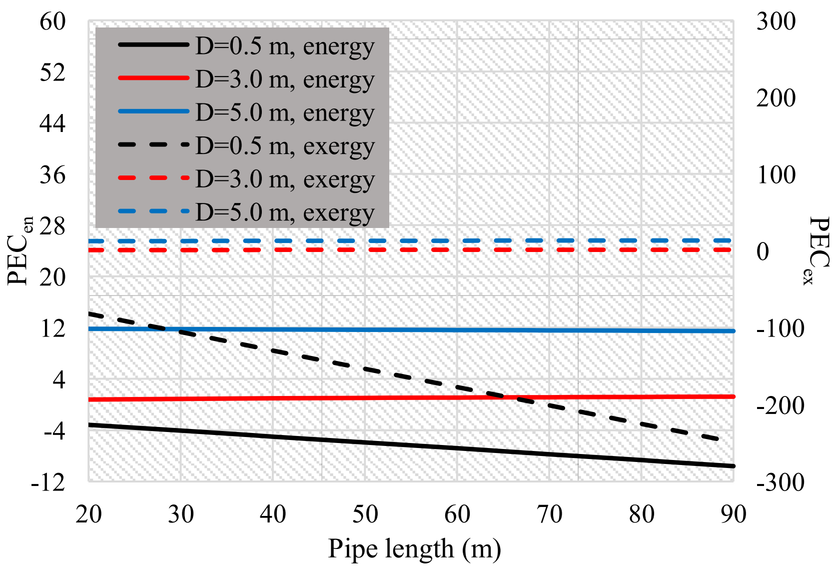

Fig. 16. The variation of yearly average PEC_{en} and PEC_{ex} as a function of pipe length for different inner pipe diameters of EAHE system for the configuration B of BIPVT-EAHE system.

5. Conclusion

In this study, two novel configurations of the BIPVT-EAHE system are proposed. Both configurations are capable of preheating/precooling the outdoor air in winter/summer and generating electricity. Besides, in both configuration, the building exhaust air is utilized to cool the PV modules. The hourly, monthly, and yearly energetic and exergetic aspects of both configurations are evaluated using an in-house Matlab code for Kermanshah weather conditions. In addition, the impacts of different influential parameters on the yearly average energetic and exergetic aspects of the best configuration of the BIPVT-EAHE system are examined. The following results are achieved from the study:

- The yearly rate of thermal energy, electrical energy, and thermal exergy gained from the configuration A are respectively 3499.59, 5908.19, and 55.59 kWh, while these values for the configuration B are respectively 3468.16, 5969.87, and 51.76 kWh.
- The yearly average PEC_{en} and PEC_{ex} of the configuration A are respectively 5.81 and 121.14, while these values for the configuration B are respectively 5.85 and 121.51. Therefore, the configuration B presents better energetic performance than the configuration A whereas the exergetic performance of the configuration A is better than the configuration B.
- Both the annual average PEC_{en} and PEC_{ex} of the BIPVT-EAHE system increase by boosting the duct length and duct width.
- Intensifying the air mass flow rate and duct depth results in a decrease in the annual average PEC_{en} and PEC_{ex} of the BIPVT-EAHE system.
- Both the annual average PEC_{en} and PEC_{ex} augment with enhancing the tube diameter of the EAHE system.

References

Agathokleous, R.A., Kalogirou, S.A., Karellas, S., 2018. Exergy analysis of a naturally ventilated Building Integrated Photovoltaic/Thermal (BIPV/T) system. Renewable Energy 128, 541-552.

Al-Ajmi, F., Loveday, D.L., Hanby, V.I., 2006. The cooling potential of earth–air heat exchangers for domestic buildings in a desert climate. Building and Environment 41, 235-244.

Al-Waeli, A.H.A., Sopian, K., Kazem, H.A., Chaichan, M.T., 2017. Photovoltaic/Thermal (PV/T) systems: Status and future prospects. Renewable and Sustainable Energy Reviews 77, 109-130.

Barbier, E., 1997. Nature and technology of geothermal energy: A review. Renewable and Sustainable Energy Reviews 1, 1-69.

Benemann, J., Chehab, O., Schaar-Gabriel, E., 2001. Building-integrated PV modules. Solar Energy Materials and Solar Cells 67, 345-354.

Bisoniya, T.S., Design of earth-air heat exchanger system. Geothermal Energy 3, 18.

Bojic, M., Trifunovic, N., Papadakis, G., Kyritsis, S., 1997. Numerical simulation, technical and economic evaluation of air-to-earth heat exchanger coupled to a building. Energy 22, 1151-1158.

Brogren, M., Nostell, P., Karlsson, B., 2001. Optical efficiency of a PV-thermal hybrid CPC module for high latitudes. Solar Energy 69, 173-185.

Chow, T.T., Hand, J.W., Strachan, P.A., 2003. Building-integrated photovoltaic and thermal applications in a subtropical hotel building. Applied Thermal Engineering 23, 2035-2049.

Chow, T.T., Chan, A.L.S., Fong, K.F., Lin, Z., He, W., Ji, J., 2009. Annual performance of building-integrated photovoltaic/water-heating system for warm climate application. Applied Energy 86, 689-696.

Chu, S., Cui, Y., Liu, N., 2016. The path towards sustainable energy. Nature Materils 16, 16.

De Paepe, M., Janssens, A., 2003. Thermo-hydraulic design of earth-air heat exchangers. Energy and buildings 35, 389-397.

Duffie, J.A., Beckman, W.A., 2013. Solar engineering of thermal processes: John Wiley & Sons.

IEA Online Data Services (https://www.iea.org/buildings/).

Jakhar, S., Soni, M.S., Boehm, R., 2018. Thermal Modeling of a Rooftop Photovoltaic/Thermal System With Earth Air Heat Exchanger for Combined Power and Space Heating, Journal of Solar Energy Engineering 140, 031011.

Jakhar, S., Soni, M.S., Gakkhar, N., 2016. Performance Analysis of Earth Water Heat Exchanger for Concentrating Photovoltaic Cooling. Energy Procedia 90, 145-153.

Jakhar, S., Soni, M.S., Gakkhar, N., 2017. Modelling and Simulation of Concentrating Photovoltaic System with Earth Water Heat Exchanger Cooling. Energy Procedia 109, 78-85.

Kasaeian, A., Khanjari, Y., Golzari, S., Mahian, O., Wongwises, S., 2017. Effects of Forced Convection on the Performance of a Photovoltaic Thermal System: An Experimental study. Experimental Thermal and Fluid Science 85, 13-21.

Khaki, M., Shahsavar, A., Khanmohammadi, S., Salmanzadeh, M., 2017. Energy and exergy analysis and multi-objective optimization of an air based building integrated photovoltaic/thermal (BIPV/T) system. Solar Energy 158, 380-395.

Khanmohammadi, S., Shahsavar, A., 2018. Energy analysis and multi-objective optimization of a novel exhaust air heat recovery system consisting of an air-based building integrated photovoltaic/thermal system and a thermal wheel. Energy Conversion and Management 172, 595-610.

Lund, J.W., Boyd, T.L., 2016. Direct utilization of geothermal energy 2015 worldwide review. Geothermics 60, 66-93.

Mahdavi, S., Sarhaddi, F., Hedayatizadeh, M., 2019. Energy/exergy based-evaluation of heating/cooling potential of PV/T and earth-air heat exchanger integration into a solar greenhouse, Applied Thermal Engineering 149, 996-1007.

Nayak, S., Tiwari, G.N., 2010. Energy metrics of photovoltaic/thermal and earth air heat exchanger integrated greenhouse for different climatic conditions of India. Applied Energy 87, 2984-2993.

Norton, B., Eames, P.C., Mallick, T.K., Huang, M.J., McCormack, S.J., Mondol, J.D., Yohanis, Y.G., 2011. Enhancing the performance of building integrated photovoltaics. Solar Energy 85, 1629-1664.

Prapas, D.E., Norton, B., Probert, S.D., 1987. Thermal design of compound parabolic concentrating solar-energy collectors. Journal of Solar Energy Engineering 109, 161-168.

Shahsavar, A., Khanmohammadi, S., Khaki, M., Salmanzadeh, M., 2018. Performance assessment of an innovative exhaust air energy recovery system based on the PV/T-assisted thermal wheel. Energy 162, 682-696.

Shahsavar, A., Rajabi, Y., 2018. Exergoeconomic and enviroeconomic study of an air based building integrated photovoltaic/thermal (BIPV/T) system. Energy 144, 877-886.

Shahsavar, A., Talebizadeh, P., Tabaei, H., 2013. Optimization with genetic algorithm of a PV/T air collector with natural air flow and a case study. Journal of Renewable and Sustainable Energy 5, 023118.

Tan, H., Charters, W., 1969. Effect of thermal entrance region on turbulent forced-convective heat transfer for an asymmetrically heated rectangular duct with uniform heat flux. Solar Energy 12, 513-516.

Tiwari, G.N., Meraj, M.D., Khan, M.E., Mishra, R.K., Garg, V., 2018. Improved Hottel-Whillier-Bliss equation for N-photovoltaic thermal-compound parabolic concentrator (N-PVT-CPC) collector, Solar Energy 166, 203-212.

Tiwari, G.N., Meraj, Khan, M.E., 2018. Exergy analysis of N-photovoltaic thermal-compound parabolic concentrator (N-PVT-CPC) collector for constant collection temperature for vapor absorption refrigeration (VAR) system. Solar Energy 173, 1032-1042.

Tonui, J., Tripanagnostopoulos, Y., 2007. Improved PV/T solar collectors with heat extraction by forced or natural air circulation. Renewable energy 32, 623-637.

Wu, J., Zhang, X., Shen, J., Wu, Y., Connelly, K., Yang, T., Tang L., Xiao, M., Wei, Y., Jiang, K., Chen, C., Xu, P., Wang, H., 2017. A review of thermal absorbers and their integration methods for the combined solar photovoltaic/thermal (PV/T) modules. Renewable and Sustainable Energy Reviews 75, 839-854.

Energy and exergy analysis of two novel hybrid solar photovoltaic geothermal energy systems incorporating a building integrated photovoltaic thermal system and an earth air heat exchanger system

Masoud Afrand[1,2], Amin Shahsavar[3], Pouyan Talebizadeh Sardari[4], Kamaruzzaman Sopian[5,*], Hamzeh Salehipour[6]

[1]Laboratory of Magnetism and Magnetic Materials, Advanced Institute of Materials Science, Ton Duc Thang University, Ho Chi Minh City, Vietnam

[2]Faculty of Applied Sciences, Ton Duc Thang University, Ho Chi Minh City, Vietnam

[3]Department of Mechanical Engineering, Kermanshah University of Technology, Kermanshah, Iran

[4]Faculty of Engineering, University of Nottingham, University Park, Nottingham, United Kingdom

[5] Solar Energy Research Institute, Universiti Kebangsaan Malaysia, Bangi, Malaysia

[6] Department of Mechanical Engineering, Ilam University, Ilam 69315-516, Iran

* Corresponding author

Emails: ksopian@ukm.edu.my; masoud.afrand@tdtu.edu.vn

Abstract

In this paper, two novel configurations of the building integrated photovoltaic thermal (BIPVT)-compound earth-air heat exchanger (EAHE) system are proposed. Both the configurations operate in two modes, namely heating and cooling modes. In the heating mode of the configuration A, the cold outdoor air is twice preheated by passing through the EAHE and BIPVT systems. In the cooling mode of the configuration A, the hot outdoor air is precooled by flowing inside the EAHE system and the PV modules are cooled using the building exhaust air. The cooling mode of the configuration B is similar to the configuration A, while in the heating mode of the configuration B, the outdoor air first enters the BIPVT collector and then passes through the EAHE system. The energetic and exergetic performances of the configurations are investigated for climatic conditions of Kermanshah, Iran. In addition, the impacts of length, width, and depth of air duct located underneath the PV panels, air mass flow rate, length and inner diameter of the pipe of EAHE system on the annual average energetic and exergetic aspects of the best configuration of the BIPVT-EAHE system are evaluated. The outcomes revealed that the annual rate of thermal energy, electrical energy, and thermal exergy captured from the configuration A are respectively 3499.59, 5908.19, and 55.59 kWh, while these values for the configuration B are respectively 3468.16, 5969.87, and 51.76 kWh. In addition, it was found that the configuration A has superior energetic performance than the configuration B, while the overall exergetic performance of the configuration B is higher than the configuration A. Furthermore, it was depicted that both the energetic and exergetic performances of the suggested configurations intensify by augmenting the duct length, duct width, and tube diameter whereas they decline with an increase in the air mass flow rate and duct depth.

Key words: Building integrated photovoltaic thermal (BIPVT); Earth-air heat exchanger (EAHE); Energy; Exergy.

Nomenclature

A	heat exchange surface area of the EAHE system (m^2)
c_p	specific heat capacity of air (J kg^{-1} K^{-1})
$D_{H,BIPVT}$	hydraulic diameter of the BIPVT collector (m)
$D_{i,EAHE}$	inner diameter of the EAHE system (m)
$\dot{E}$	electric power generated by the BIPVT-EAHE system (kWh)
$\dot{E}_{fan,BIPVT}$	electric power consumed by fans to blow air inside the BIPVT collector (kWh)

$\dot{E}_{BIPVT,net}$	net electric power gained from the BIPVT collector (kWh)
$\dot{E}_{EAHE}$	electric power consumption of the EAHE system (kWh)
f_{BIPVT}	fanning friction factor for the BIPVT collector
f_{EAHE}	fanning friction factor for the EAHE system
h	convective heat exchange coefficient of the EAHE system (W K^{-1} m^{-2})
h_c	convective heat exchange coefficient of the BIPVT collector (W K^{-1} m^{-2})
$h_{r,pv-b}$	radiative heat exchange coefficient between the PV modules and back wall (W $K^{-1}m^{-2}$)
$h_{r,pv-s}$	radiative heat exchange coefficient between the PV modules and sky (W $K^{-1}m^{-2}$)
h_w	wind convective heat exchange coefficient (W $K^{-1}m^{-2}$)
I_r	intensity of solar radiation (W m^{-2})
k	thermal conductivity (W m^{-1} K^{-1})
$k_{c,BIPVT}$	loss coefficient of the BIPVT collector
$k_{c,EAHE}$	loss coefficients of the EAHE system
k_{ins}	thermal conductivity of insulation material (W $m^{-1}K^{-1}$)
L	length of the PV duct (m)
L_{EAHE}	Length of the EAHE system (W $m^{-1}K^{-1}$)
$\dot{m}_f$	air mass flow rate (kg s^{-1})
NTU	number of transfer units
ΔP	frictional pressure loss (Pa)
ΔP_{BIPVT}	frictional pressure loss in BIPVT collector (Pa)
ΔP_{EAHE}	frictional pressure loss in EAHE system (Pa)
$\mathrm{PEC_{en}}$	energetic performance evaluation criterion

PEC_{ex}	exergetic performance evaluation criterion
Pr	Prandtl number
$\dot{Q}$	thermal power gained from the BIPVT-EAHE system (kWh)
$\dot{Q}_{BIPVT}$	thermal power gained from the BIPVT collector (kWh)
$\dot{Q}_{EAHE}$	thermal power gained from the EAHE system (kWh)
$\dot{Q}_{EAHE,max}$	maximum possible thermal power gained from the EAHE system (kWh)
Re_{BIPVT}	Reynolds number of the BIPVT collector
Re_{EAHE}	Reynolds number of the EAHE system
S	depth of the PV duct (m)
T_a	outdoor air temperature (K)
T_b	back wall temperature (K)
T_f	air temperature (K)
T_{in}	temperature of inlet air through the PV duct (K)
$T_{in,EAHE}$	temperature of inlet air through the EAHE system (K)
T_{mf}	mean air temperature inside the PV duct (K)
$T_{out,EAHE}$	temperature of outlet air from the EAHE system (K)
T_{pv}	PV module temperature (K)
T_s	sky temperature (K)
T_{soil}	soil temperature (K)
U_b	bottom heat loss coefficient (W $K^{-1}m^{-2}$)
v_w	wind speed (m s^{-1})
W	width of the PV duct (m)
$\dot{X}_{dest,BIPVT}$	exergy loss from the BIPVT collector (kWh)
$\dot{X}_{dest,EAHE}$	exergy loss from the EAHE system (kWh)

$\dot{X}_{el}$	electrical exergy gained from the BIPVT-EAHE system (kWh)
$\dot{X}_{el,BIPVT}$	electrical exergy gained from the BIPVT system (kWh)
$\dot{X}_{el,EAHE}$	electrical exergy gained from the EAHE system (kWh)
$\dot{X}_{el,PV}$	electrical exergy of the PV modules (kWh)
$\dot{X}_{fan,BIPVT}$	exergy of fan consumed power in the BIPVT collector (kWh)
$\dot{X}_{fan,EAHE}$	exergy of fan consumed power in the EAHE system (kWh)
$\dot{X}_{in,BIPVT}$	exergy of air entering the BIPVT collector (kWh)
$\dot{X}_{in,EAHE}$	exergy of air entering the EAHE system (kWh)
$\dot{X}_{out,BIPVT}$	exergy of air leaving the BIPVT collector (kWh)
$\dot{X}_{out,EAHE}$	exergy of air leaving the EAHE system (kWh)
$\dot{X}_{th}$	thermal exergy gained from the BIPVT-EAHE system (kWh)
$\dot{X}_{th,BIPVT}$	thermal exergy gained from the BIPVT system (kWh)
$\dot{X}_{th,EAHE}$	thermal exergy gained from the EAHE system (kWh)

Greek symbols

α_{pv}	absorptance of PV modules
μ	air viscosity (kg m^{-1} s^{-1})
δ_{ins}	thickness of insulation material (m)
ε	effectiveness of EAHE system
ε_b	emissivity of back wall
ε_{pv}	emissivity of PV module
η_{el}	electrical conversion efficiency of PV modules
η_{fan}	fan efficiency

ρ	air density (kg m^{-3})
σ	Stefan-Boltzmann constant (5.67×10^{-8} W m^{-2} K^{-4})

1. Introduction

According to the International Energy Agency (IEA), 36% of the global final energy consumption is accounted by buildings and buildings construction sector which are also responsible for 40% of total direct and indirect CO_2 emissions (IEA, 2019). In the buildings, the rate of increase in global energy usage and CO_2 emission are both 1% each year (IEA, 2019). Buildings also account for more than 55% of the global electricity demand which increases with the yearly rate of 2.5% (IEA, 2019). To decrease the huge amount of direct and indirect CO_2 emissions, the use of renewable energies have been recommended (Chu et al., 2016).

Photovoltaic (PV) systems have been widely used for generating electricity in the world. The amount of electricity produced by PV modules accounts for 2.1% of the global electricity demand equals to 401 GW which increases by 34% growth year-on-year of new installations (Chu et al., 2016). In buildings, the PV modules can be used directly for electricity generation to provide a part of the required electricity. However, the efficiency of the modules reduces by boosting their temperature (Prapas et al., 1987; Brogren et al., 2001; Wu et al., 2017). A possible attractive option which results in the simultaneous production of electricity and heat as well as the enhancement of the PV efficiency is the employment of PVT systems (Norton et al., 2011). In the PVT collectors, a PV module and a heat exchanger are combined as an integrated system which provides a sustainable solution for the built environment (Benemann et al., 2001; Tiwari et al., 2018; Tiwari et al., 2018). The heat exchanger is responsible to gain heat from the PV module to reduce its temperature. The gained thermal energy can also be utilized for heating/cooling purposes in buildings which shows a great potential in HVAC systems (Al-Waeli et al., 2017). Chow et al. (2003) examined a large scale BIPVT system in a subtropical hotel in China. They simulated the performance of the system using ESP-r building energy simulation software and showed the improved electrical efficiency of the system. Furthermore, they utilized the gained heat to decrease the heating load of building. Chow et al. (2009) studied the energy matrices of a water-cooled BIPVT collector for Hong Kong climatic conditions. After presenting the advantages of the proposed system, they reported the yearly thermal and PV module efficiencies of 37.5% and 9.39%, respectively. Shahsavar et al. (2013, 2018) proposed a novel BIPVT collector to provide a part of the heating load of a building as well as cool the PV modules. The gained heat from the PV modules was then used to preheat the outdoor air. They reported that the annual electrical and thermal energy savings potential of the system is respectively 178.2 kWh and 3400.4 kWh. Agathokleous et al. (2018) evaluated the energetic and exergetic performances of a naturally ventilated BIPVT collector. They showed the energy and exergy efficiencies of the system are in the range of 26.5-33.5% and 13-16%, respectively.

Geothermal energy is attractive as an energy source mainly because of its enormous potential and ability to provide base-load power (Lund and Boyd, 2016). In contrast to wind and solar energies that are dependent on the weather conditions and time of day and year, the geothermal system is not restricted to specific countries and can provide energy anywhere in the world. The earth's constant temperature makes geothermal systems as one of the most efficient for heating/cooling purpose (Barbier, 1997). For air heating and cooling, geothermal energy can be used directly by forwarding the cold/warm air to the earth in winter/summer to provide warm/cold air for heating/cooling purposes. It can also be used by a second heat transfer fluid in a heat exchanger indirectly. Due to the significant advantages of the geothermal energy, several researchers have been attracted to use the earth as a heat source to provide all or a part of the heating/cooling load. Bojic et al. (1997) numerically studied an

EAHE integrated with a building using 100% fresh air for heating/cooling purposes and proved that the system could provide a noticeable part of the heating/cooling load of the building. Al-Ajmi et al. (2006) developed a theoretical model to forecast the outlet temperature of an EAHE for cooling purposes in a hot, arid climate. The building simulation was also performed using TRNSYS software and showed a 30% reduction of the cooling energy demand over the peak summer season. The EAHE showed a cooling load reduction of 1700 W with an indoor temperature reduction of 2.8 °C. Jakhar et al. (2016) simulated an earth-water heat exchanger (EWHE) for India using TRNSYS software. They performed a parameter study and compared the findings with an existed concentrating PV (CPV) system. The better performance of the proposed EWHE system was reported as compared with the CPV system using a pipe length of 60 m in the depth of 3.5 m for pipe burial.

Recently, hybrid renewable systems have attracted significant attention due to the simultaneous use of different renewable energies. The hybrid usage of PVT integrated with EAHE to provide required electricity and heating/cooling load of a building is rarely discussed in the literature (Nayak and Tiwari, 2010; Jakhar et al., 2018; Mahdavi et al., 2019). Nayak and Tiwari (2010) studied the performance of an integrated PVT-EAHE system for a greenhouse for various climatic conditions of India. In their system, both the PVT and EAHE systems were used to preheat the air entering the greenhouse. The outcomes showed that Jodhpur is the best place due to greater solar intensity. Jakhar et al. (2018) numerically assessed the thermal performance of a PVT-EAHE system for climatic conditions of Pilani, Ajmer (India) and Las Vegas (USA). The system was able to preheat the cold ambient air by passing it through the PVT and EAHE systems and generate electricity. The heating capacity of the EAHE was observed to be augmented with PVT system by 0.024 kWh to 0.299 kWh, 0.071 kWh to 0.316 kWh and 0.041 kWh to 0.271 kWh for the Pilani, Ajmer and Las Vegas, respectively. Mahdavi et al. (2019) theoretically evaluated the energetic and exergetic performances of a PVT-EAHE system integrated into a solar greenhouse. In the proposed system, the greenhouse air was preheated/precooled by passing through the EAHE system and returned back to the greenhouse. Air inside the greenhouse was also preheated by passing it through the channel located under the PV panels. The results revealed that the PVT system was not able to considerably preheat the greenhouse air. However, the hybrid PVT-EAHE seemed promising in preheating/precooling the greenhouse air by 9 °C and 8 °C in summer/winter, respectively.

The aim of this paper is to analyse the performance of two novel configurations of the BIPVT-EAHE system for climatic conditions of Kermanshah, Iran. Both configurations are able to preheat/precool the outdoor air and generate electricity. In addition, these innovative configurations utilize the building exhaust air to cool the PV panels during the warm months. To the best of our knowledge, the use of exhaust air in the hybrid PVT-EAHE systems has not yet been evaluated in any study. The energy and exergy analysis of the proposed configurations of the BIPVT-EAHE system are performed comprehensively. Then, the effects of different influential parameters on the energetic and exergetic aspects of the best configuration of the BIPVT-EAHE system are examined. The system is evaluated for Kermanshah city in the west of Iran (34.33°N, 47.08°E) with relatively high annual solar radiation of about 7045 MJ/m^2 based on the Iranian Meteorological Organization (IMO) (Khaki et al., 2017).

2. System description

Figs. 1 and 2 display the schematic sketch of the suggested configurations of the BIPVT-EAHE system. Both configurations have two modes of heating and cooling. For the first configuration (configuration A), in the heating mode, the cold outdoor air enters the EAHE system where it is preheated by receiving the heat from the surrounding soil. Then, this preheated air enters the BIPVT collector and is preheated again by absorbing the surplus thermal energy of the PV modules. This results in the cooling of PV modules and consequently, their electrical efficiency augments. In the cooling mode of the first configuration, the hot outdoor air is precooled by transferring heat to the surrounding soil. Besides, the building exhaust air is passed through the duct located underneath the PV modules and thereby reduces their temperature and increases their efficiency. As Fig. 2 shows, for the second configuration (configuration B), in the heating mode, the outdoor air enters the BIPVT collector and then passes through the EAHE system. This causes the air passing through the BIPVT collector to be cooler in the second configuration than in the first configuration and, therefore, the modules are better cooled in the second configuration. Conversely, the temperature difference between the air entering the EAHE system and soil temperature is less in the second configuration than in the first; which leads to lower efficiency of the EAHE system in the second configuration. Additionally, it is seen that the cooling mode of operation is the same for both configurations. It should be noted that both configurations generates electricity, part of which consumes by fans to circulate air through the BIPV/T and EAHE systems, and the rest can cover part of the electricity demand of the building.

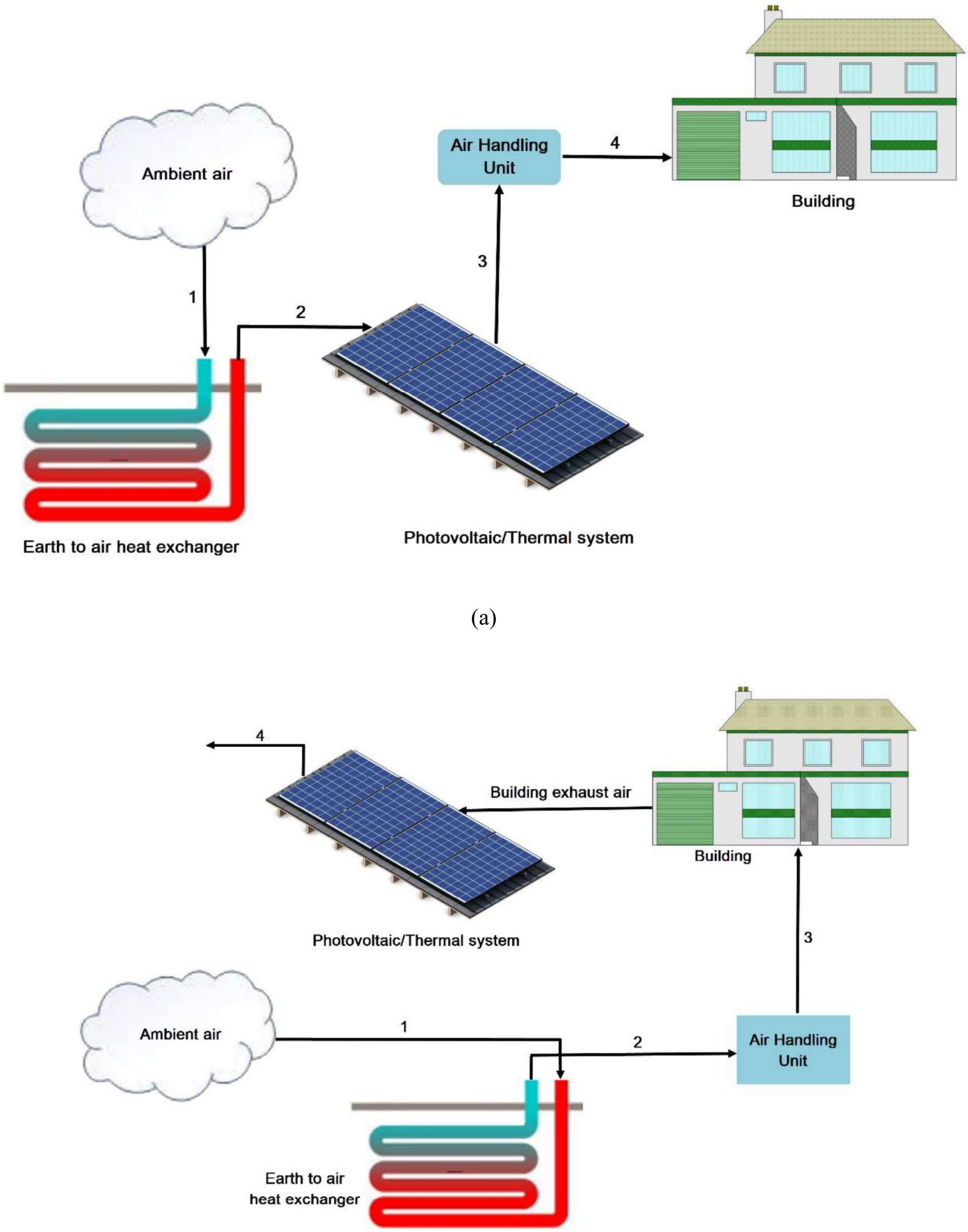

(a)

(b)

Fig. 1. The working concept of the configuration A: (a) heating mode and (b) cooling mode.

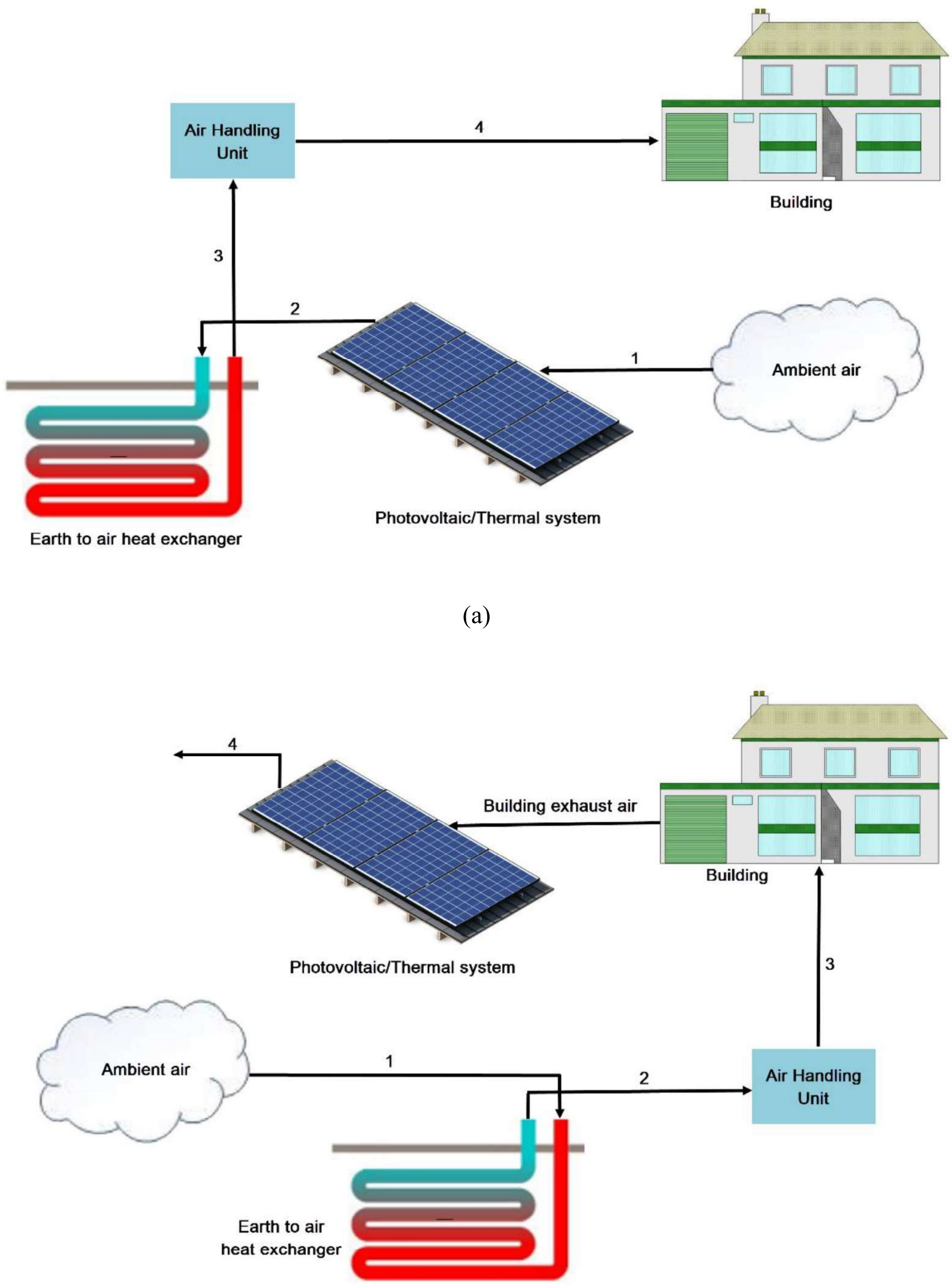

(a)

(b)

Fig. 2. The working concept of the configuration B: (a) heating mode and (b) cooling mode.

3. Mathematical Modelling

3.1. BIPVT collector

The energy balance equations for different layers of the PVT collector are written under the following assumptions (Khaki et al., 2017):

(1) Heat transfer is one-dimensional steady-state.

(2) Convection heat transfer coefficient is constant over the entire duct.

(3) Temperature is uniform over the PV module and back insulation surface.

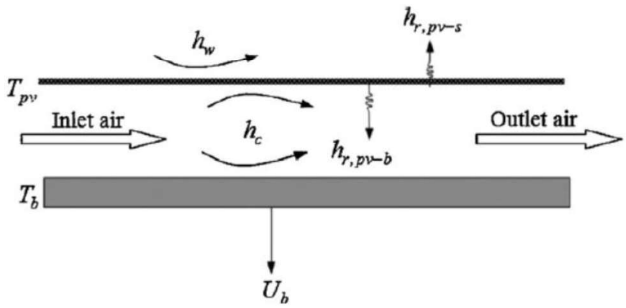

Fig. 3. The Schematic view of the suggested PVT collector.

Therefore, the energy balance equations are as follows (Shahsavar and Rajabi, 2018; Khaki et al., 2017):

For PV modules:

$$\alpha_{pv}(1-\eta_{el})I_r W dx = \left(h_{r,pv-s}+h_w\right)\left(T_{pv}-T_a\right)W dx + h_c\left(T_{pv}-T_f\right)W dx + h_{r,pv-b}\left(T_{pv}-T_b\right)W dx \quad (1)$$

For air stream:

$$\dot{m}_f c_p dT_f = h_c\left(T_{pv}-T_f\right)W dx + h_c(T_b-T_f)W dx \quad (2)$$

For back insulation surface:

$$h_{r,pv-b}\left(T_{pv}-T_b\right)W dx = U_b(T_b-T_a)W dx + h_c\left(T_b-T_f\right)W dx \quad (3)$$

From Eqs. (1) and (3), Eq. (2) can be written as follows:

$$\frac{dT_f}{dx} + A_1 T_f = A_2 \quad (4)$$

where

$$\mathrm{A}_1 = \frac{h_c W}{\dot{m}_f c_p}\ (2 - \mathrm{A}_{1-1} - \mathrm{A}_{1-2}) \tag{5a}$$

$$\mathrm{A}_{1-1} = \frac{(h_c + (\ h_{r,pv-b} h_c / h_{r,pv-b} + U_b + h_c))/\ h_w + h_{r,pv-s} + h_c + h_{r,pv-b}}{1 - (h_{r,pv-b}^2\ /\ (h_w + h_{r,pv-s} + h_c + h_{r,pv-b})(h_{r,pv-b} + U_b + h_c))} \tag{5b}$$

$$\mathrm{A}_{1-2} = \frac{\dfrac{h_{r,pv-b}((h_c + (\ h_{r,pv-b} h_c / (h_{r,pv-b} + U_b + h_c)))/\ (h_w + h_{r,pv-s} + h_c + h_{r,pv-b}))}{1 - (h_{r,pv-b}^2\ /\ (h_w + h_{r,pv-s} + h_c + h_{r,pv-b})(h_{r,pv-b} + U_b + h_c))} + h_c}{h_{r,pv-b} + U_b + h_c} \tag{5c}$$

and

$$\mathrm{A}_2 = \frac{h_c W}{\dot{m}_f c_p}\ (\mathrm{A}_{2-1} + \mathrm{A}_{2-2}) \tag{6a}$$

$$A_{2-1} = \frac{\alpha_{pv}(1 - \eta_{el}) I_r + \left(\ h_w + h_{r,pv-s}\right) T_a + \dfrac{\left(\dfrac{h_{r,pv-b} U_b T_a}{h_{r,pv-b}\ +\ U_b + h_c}\right)}{h_w + h_{r,pv-s} +\ h_c + h_{r,pv-b}}}{1 - (h_{r,pv-b}^2\ /\ (h_w + h_{r,pv-s} + h_c + h_{r,pv-b})(h_{r,pv-b} + U_b + h_c))} \tag{6b}$$

$$A_{2-2} = \frac{\dfrac{h_{r,pv-b} \dfrac{\alpha_{pv}(1 - \eta_{el}) I_r + \left(\ h_w + h_{r,pv-s}\right) T_a + \dfrac{h_{r,pv-b} U_b T_a}{h_{r,pv-b} + U_b\ + h_c}}{h_w + h_{r,pv-s} + h_c + h_{r,pv-b}}}{1 - (h^2{}_{r,pv-b}\ /\ (h_w + h_{r,pv-s} + h_c + h_{r,pv-b})(h_{r,pv-b} + U_b + h_c))} + U_b T_a}{h_{r,pv-b} + U_b + h_c} \tag{6c}$$

By using boundary condition (i.e. $T_f\big|_{x=0} = T_{in,BIPV/T}$), T_f is obtained as:

$$T_f(x) = \left(\ T_{in,BIPV/T} - \frac{A_2}{A_1}\right) e^{-A_1 x} + \frac{A_2}{A_1} \tag{7}$$

which results in the outlet air temperature of:

$$T_f(L) = \left(\ T_{in,BIPV/T} - \frac{A_2}{A_1}\right) e^{-A_1 L} + \frac{A_2}{A_1} \tag{8}$$

The average air temperature is given as:

$$T_{mf} = \frac{1}{L}\int_{0}^{L} T_f(x)\, dx = \left(T_{in,BIPV/T} - \frac{A_2}{A_1}\right)\frac{1}{A_1}(1 - e^{-A_1 L}) + \frac{A_2}{A_1}L \tag{9}$$

By using the average air temperature, the PV modules and back insulation temperatures are calculated as:

$$T_{pv} = A_{2-1} + A_{1-1}T_{mf} \tag{10}$$

$$T_b = A_{2-2} + A_{1-2}T_{mf} \tag{11}$$

The wind-induced exterior heat exchange coefficient is computed as (Duffie and Beckman, 2013):

$$h_w = 2.8 + 3v_w, \qquad v_w < 7 \text{ m/s} \tag{12}$$

where v_w is the wind velocity.

The convective heat transfer coefficient of air inside the duct is obtained as (Tan and Charters, 1969):

$$h_c = \frac{k}{D_{H,BIPVT}}\left\{0.0182 {Re_{BIPVT}}^{0.8} Pr^{0.4}\left[1 + j\frac{D_{H,BIPVT}}{L}\right]\right\} \tag{13}$$

$$\begin{aligned} j &= 14.3\log\left(\frac{L}{D_{H,BIPVT}}\right) - 7.9 \quad \text{for} \quad 0 < \frac{L}{D_{H,BIPVT}} \le 60 \\ &= 17.5 \quad \text{for} \quad \frac{L}{D_{H,BIPVT}} > 60 \end{aligned} \tag{14}$$

where k is the thermal conductivity of air and $D_{H,PV/T}$ is the hydraulic diameter of the duct below the PV modules ($= 2WS/(W + S)$).

The radiative heat exchange coefficient between the PV modules and sky is calculated as (Khaki et al., 2017; Duffie and Beckman, 2013):

$$h_{r,pv-s} = \sigma\varepsilon_{pv}\frac{\left(T_{pv}^4 - T_s^4\right)}{T_{pv} - T_a} \tag{15}$$

where T_s is the equivalent sky temperature given as (Duffie and Beckman, 2013):

$$T_s = 0.0552T_a^4 \tag{16}$$

The radiative heat exchange coefficient between the PV modules and back wall is calculated as (Duffie and Beckman, 2013):

$$h_{r,pv-b} = \sigma(T_{pv} + T_b)(T_{pv}^2 + T_b^2)\left(\frac{1}{\varepsilon_{pv}} + \frac{1}{\varepsilon_b} - 1\right) \quad (17)$$

For the conduction losses through the back insulation layer, the bottom heat loss coefficient is given as (Khaki et al., 2017):

$$U_b = \frac{k_{ins}}{\delta_{ins}} \quad (18)$$

where k_{ins} is the thermal conductivity of the insulation material and δ_{ins} is the thickness of the insulation material.

3.2. EAHE system

In the earth-air heat exchanger, the heat is transferred to/from the air flows through the pipe walls in the earth by convection and from pipe walls to the surrounding soil and vice versa by conduction. Effectiveness-number of transfer units ($\varepsilon - \mathrm{NTU}$) method is used to evaluate the heat transfer performance of the EAHE system defined as the ratio of the actual heat transfer to the maximum possible heat transfer (Bisoniya, 2015):

$$\varepsilon = \frac{\dot{Q}_{EAHE}}{\dot{Q}_{EAHE,max}} = \frac{T_{out,EAHE} - T_{in,EAHE}}{T_{soil} - T_{in,EAHE}} \quad (19)$$

where $T_{in,EAHE}$ is the inlet air temperature, $T_{out,EAHE}$ is the outlet air temperature of , and T_{soil} is the soil temperature. The temperature of earth at a depth of 1.5 to 2 m remains fairly constant throughout the year called earth's undisturbed temperature (EUT) (De Paepe and Janssens, 2003). The EUT temperature is defined as the yearly mean outdoor air temperature of a specific location which is equals to 295.3 K for Kermanshah, Iran (Khaki et al., 2017).

The effectiveness is also calculated as (Bisoniya, 2015):

$$\varepsilon = 1 - exp(-\mathrm{NTU}) \quad (20)$$

where NTU is the number of transfer units given as (Bisoniya, 2015):

N (21)

and A is the surface area of heat transfer given as:

$$A = \pi D_{i,EAHE} L_{EAHE} \quad (22)$$

Here, $D_{i,EAHE}$ and L_{EAHE} respectively denote the inner diameter and length of EAHE system. In Eq. (21), h is the convective heat exchange coefficient determined as (De Paepe and Janssens, 2003):

$$h = 3.66 \frac{k}{D_{i,EAHE}} \qquad \text{if } Re_{EAHE} < 2300 \quad (23a)$$

$$h = \frac{k}{D_{i,EAHE}} \left[\frac{(\xi/8)(Re_{EAHE} - 1000)Pr}{1 + 12.7\sqrt{\xi/8}(Pr^{2/3} - 1)} \right] \qquad if\ 2300 \leq Re_{EAHE} < 5 \times 10^6 \quad (23a)$$

where

$$\xi = (1.82 \log Re_{EAHE} - 1.64)^{-2} \qquad \text{if } Re_{EAHE} > 2300 \quad (24)$$

The effectiveness is computed by applying Eqs. (20)-(24) which is then used to calculate the outlet air temperature as:

$$T_{out,EAHE} = T_{in,EAHE} + \varepsilon(T_{soil} - T_{in,EAHE}) \quad (25)$$

3.3. Performance evaluation

For the fresh air, the rate of thermal energy received from the system is obtained as:

$$\dot{Q} = \dot{Q}_{BIPV/T} + \dot{Q}_{EAHE} \quad (26)$$

where

$$\dot{Q}_{BIPV/T} = \dot{m}_f c_p \left[T_f(L) - T_{in} \right] \quad (27)$$

$$\dot{Q}_{EAHE} = \dot{m}_f c_p (T_{out,EAHE} - T_{in,EAHE}) \quad (28)$$

The rate of produced electricity by the BIPVT-EAHE system is given as:

$$\dot{E} = \dot{E}_{BIPV/T,net} - \dot{E}_{EAHE} \tag{29}$$

where

$$\dot{E}_{BIPVT,net} = \alpha_{pv}\eta_{el}I_r WL - \dot{E}_{fan,BIPVT} \tag{30}$$

$$\eta_{el} = 0.125\left[\,1 - 0.006\left(T_{pv} - 298\right)\right] \tag{31}$$

where $\dot{E}_{fan,BIPVT}$ and $\dot{E}_{EAHE}$ are respectively the fan consumed power to blow air inside the BIPVT and EAHE systems, which are obtained using the following equation (Khaki et al., 2017):

$$\dot{E}_{fan} = \frac{(\dot{m}_f/\rho)\Delta P}{\eta_{fan}} \tag{32}$$

η_{fan} is the fan efficiency. Furthermore, ΔP is the pressure loss through the duct given as (Khanmohammadi and Shahsavar, 2018):

$$\Delta P_{BIPVT} = \frac{1}{2}k_{c,BIPVT}\frac{\dot{m}_f^2}{\rho(WS)^2} + f_{BIPVT}\frac{L}{D_{H,BIPVT}}\frac{\dot{m}_f^2}{\rho(WS)^2} \tag{33}$$

$$\Delta P_{EAHE} = \frac{1}{2}k_{c,EAHE}\frac{\dot{m}_f^2}{\rho\left(\frac{\pi}{4}D_{i,EAHE}^2\right)^2} + f_{EAHE}\frac{L_{EAHE}}{D_{i,EAHE}}\frac{\dot{m}_f^2}{\rho\left(\frac{\pi}{4}D_{i,EAHE}^2\right)^2} \tag{34}$$

where $k_{c,BIPVT}$ and $k_{c,EAHE}$ are the inlet and outlet loss coefficients for the BIPVT and EAHE systems, respectively. Moreover, f_{BIPVT} and f_{EAHE} are respectively the fanning friction factors for the BIPVT and EAHE systems, computed as (Jakhar et al., 2017):

$$f_{BIPVT} = \frac{0.079}{{Re_{BIPVT}}^{0.25}} \tag{36}$$

$$f_{EAHE} = \frac{0.079}{{Re_{EAHE}}^{0.25}} \tag{37}$$

where Re_{BIPVT} and Re_{EAHE} are the Reynolds number of air inside the BIPVT collector and EAHE, respectively, estimated as:

$$Re_{BIPVT} = \frac{\dot{m}_f D_{H,BIPVT}}{WS\mu} \tag{38}$$

$$Re_{EAHE} = \frac{4\dot{m}_f}{\pi D_{i,EAHE}\mu} \tag{39}$$

To examine the overall energetic aspect of the BIPVT-EAHE system, a new parameter called the Energetic Performance Evaluation Criterion ($\mathrm{PEC_{en}}$) is defined as the ratio of the total thermal and electrical power received from the system to the heating/cooling load of the outdoor air, given as:

$$\mathrm{PEC_{en}} = \frac{\dot{Q} + \left(\dot{E}/0.36\right)}{\dot{m}_f c_p |296 - T_a|} \tag{40}$$

where the coefficient 0.36 is the conversion factor of the thermal power plant (Shahsavar et al., 2018).

3.4. Exergy analysis

According to the Second Law of Thermodynamics, the exergy analysis of the EAHE system is given as:

$$\dot{X}_{in,EAHE} = \dot{X}_{out,EAHE} + \dot{X}_{fan,EAHE} + \dot{X}_{dest,EAHE} \tag{41}$$

In the above equations, $\dot{X}_{in,EAHE}$ is the exergy of inlet air, $\dot{X}_{out,EAHE}$ is the exergy of outlet air, $\dot{X}_{fan,EAHE}$ is the exergy of fun consumed power, and $\dot{X}_{dest,EAHE}$ is the exergy loss from the EAHE system.

The exergy of inlet and outlet air is because of the temperature and is computed as (Khaki et al., 2017):

$$\dot{X}_{in,EAHE} = \dot{m}_f c_p \left[T_{in,EAHE} - T_a - T_a \ln\left(\frac{T_{in,EAHE}}{T_a}\right)\right] \tag{42}$$

$$\dot{X}_{out,EAHE} = \dot{m}_f c_p \left[T_{out,EAHE} - T_a - T_a \ln\left(\frac{T_{out,EAHE}}{T_a}\right)\right] \tag{43}$$

The electrical energy can be completely converted into work and consequently, its exergy amount is equivalent to the energy amount of electrical flow (Khaki et al., 2017). Therefore, the fan consumed exergy is equal to the fan consumed power.

For the BIPVT collector, the exergy analysis is performed as (Khaki et al., 2017):

$$\dot{X}_{in,BIPVT} + \dot{X}_{solar} + \dot{X}_{fan,BIPVT} = \dot{X}_{out,BIPVT} + \dot{X}_{el,PV} + \dot{X}_{dest,BIPVT} \tag{44}$$

where $\dot{X}_{in,BIPVT}$, $\dot{X}_{out,BIPVT}$ and $\dot{X}_{solar}$ are respectively the exergy of inlet air, outlet air and solar light. Moreover, $\dot{X}_{fan,BIPVT}$ and $\dot{X}_{el,PV}$ are the exergy of fan consumed power and electrical exergy of the PV modules, respectively. $\dot{X}_{dest,BIPVT}$ is the exergy loss from the BIPVT system.

The exergy of inlet and outlet air streams are calculated as (Khaki et al., 2017):

$$\dot{X}_{in,BIPVT} = \dot{m}_f c_p \left[T_{in,BIPVT} - T_a - T_a \ln\left(\frac{T_{in,BIPVT}}{T_a}\right)\right] \tag{45}$$

$$\dot{X}_{out,BIPVT} = \dot{m}_f c_p \left[T_{out,BIPVT} - T_a - T_a \ln\left(\frac{T_{out,BIPVT}}{T_a}\right)\right] \tag{46}$$

The rate of thermal exergy that the fresh air gains from system is given as:

$$\dot{X}_{th} = \dot{X}_{th,BIPVT} + \dot{X}_{th,EAHE} \tag{47}$$

where

$$\dot{X}_{th,BIPVT} = \dot{m}_f c_p \left[T_{out,BIPVT} - T_{in,BIPVT} - T_a \ln\left(\frac{T_{out,BIPVT}}{T_{in,BIPVT}}\right)\right] \tag{48}$$

$$\dot{X}_{th,EAHE} = \dot{m}_f c_p \left[T_{out,EAHE} - T_{in,EAHE} - T_a \ln\left(\frac{T_{out,EAHE}}{T_{in,EAHE}}\right)\right] \tag{49}$$

The rate of electrical exergy generated by the BIPVT-EAHE system is obtained as:

$$\dot{X}_{el} = \dot{X}_{el,BIPVT} + \dot{X}_{el,EAHE} \tag{50}$$

where

$$\dot{X}_{el,BIPVT} = \alpha_{pv} \eta_{el} I_r W L - \dot{E}_{fan,BIPVT} \tag{51}$$

$$\dot{X}_{el,EAHE} = \dot{E}_{fan,EAHE} \tag{52}$$

Similar to the energy analysis, the overall exergetic performance of the system called as the Exergetic Performance Evaluation Criterion (PEC_{ex}) is defined as the ratio of the total thermal and electrical exergy gained from the system to the exergy load of the fresh air:

$$\mathrm{PEC_{ex}} = \frac{\dot{X}_{th} + \dot{X}_{el}}{\dot{m}_f c_p \left| 296 - T_a - T_a \ln\left(\frac{296}{T_a}\right) \right|} \tag{53}$$

4. Results and discussion

In this study, the presented mathematical model has been solved by following an iterative process as depicted in Fig. 4. After the model validation, the energetic and exergetic performances of the two proposed configurations for the BIPVT-EAHE system are examined. For this purpose, firstly, the hourly temperature of outlet air and PV module are presented for a typical cold day (January 15th) and a typical warm day (August 15th). Then, the rates of gained thermal energy and exergy and the net produced electric power are studied in different months for both configurations. Finally, the better system is selected and the variation of effective parameters on the energetic and exergetic performances are analysed. The constant design aspects of the system are presented in Table 1. The solar radiation intensity and outdoor air temperature for a simple day of each month for Kermanshah can be found in Ref. (Shahsavar et al., 2018).

Table 1. Design aspect of the BIPVT-EAHE system under investigation.

c_p, J/kgK	1005	S, m	0.5
$D_{i,EAHE}$, m	0.1	v_w, m/s	1.5
k, W/mK	0.0257	W, m	3
$k_{c,BIPVT}$, W/mK	1.5	α_{pv}	0.9
$k_{c,EAHE}$, W/mK	2.6	δ_{ins}, m	0.025
k_{ins}, W/mK	0.045	ε_{pv}	0.8

L_{EAHE}, m	25	η_{fan}	0.5
L, m	10	μ, kg/ms	0.00001511
$\dot{m}_f$, kg/s	0.01	ρ, kg/m^3	1.2

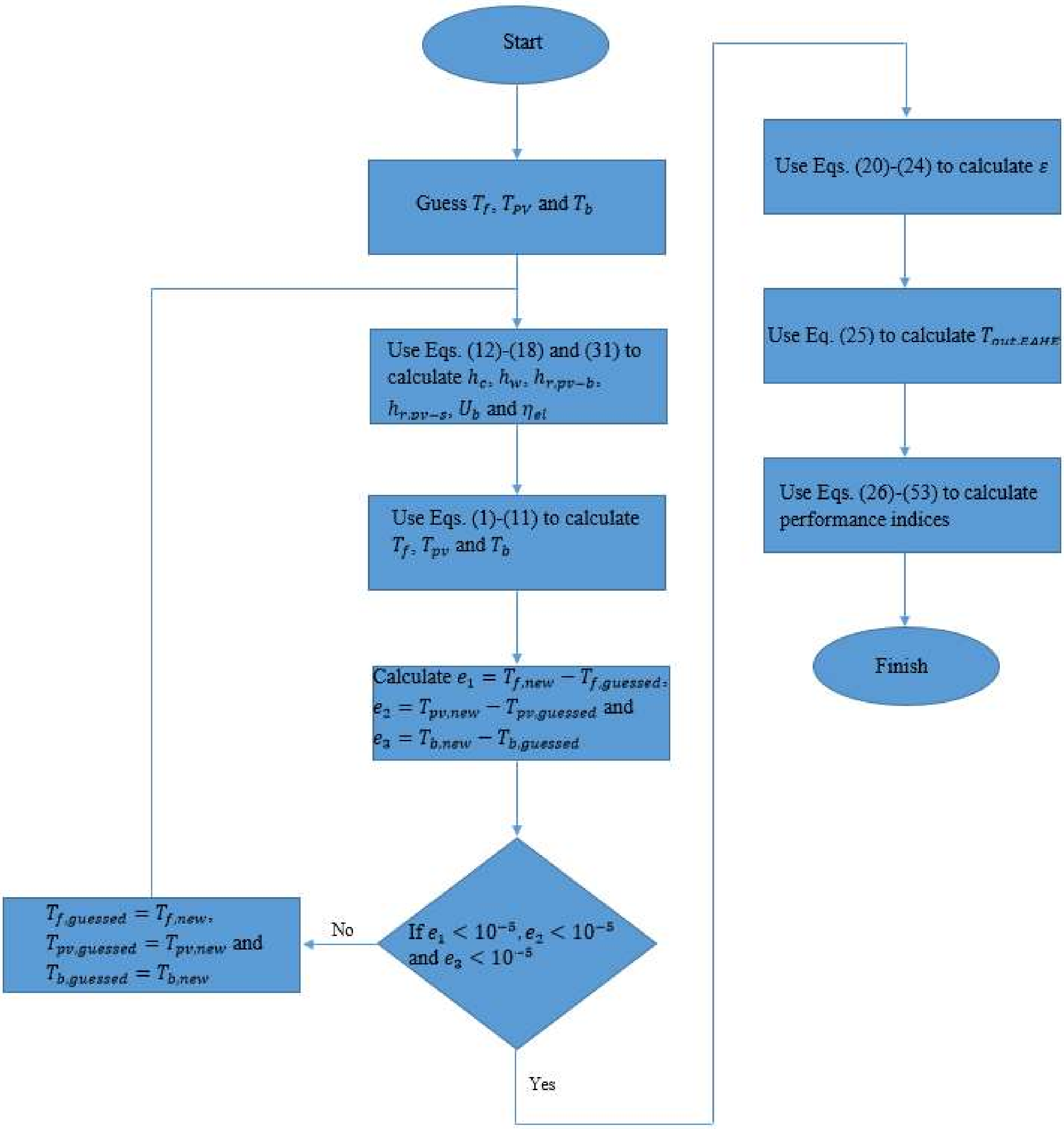

Fig. 4. Flowchart for mathematical modelling of the BIPVT-EAHE system.

4.1. Model validation

The experimental results of Tonui and Tripanagnostopoulos (2007) is employed for comparison based on the PV module temperature and the outlet air temperature. They studied a PVT including a single-pass air duct below the module. Fig. 5 illustrates the comparison of the findings of current investigation with those of Tonui and Tripanagnostopoulos (2007) presenting the accuracy of the present simulation carried out using MATLAB software. Moreover, the PV module temperature and the outlet air temperature obtained in the current study are compared to the experimental findings of Kasaeian et al. (2017) for the case of single-pass air PVT system. This comparison is illustrated in Fig. 6, and it can be observed that there is a suitable consistency between the results.

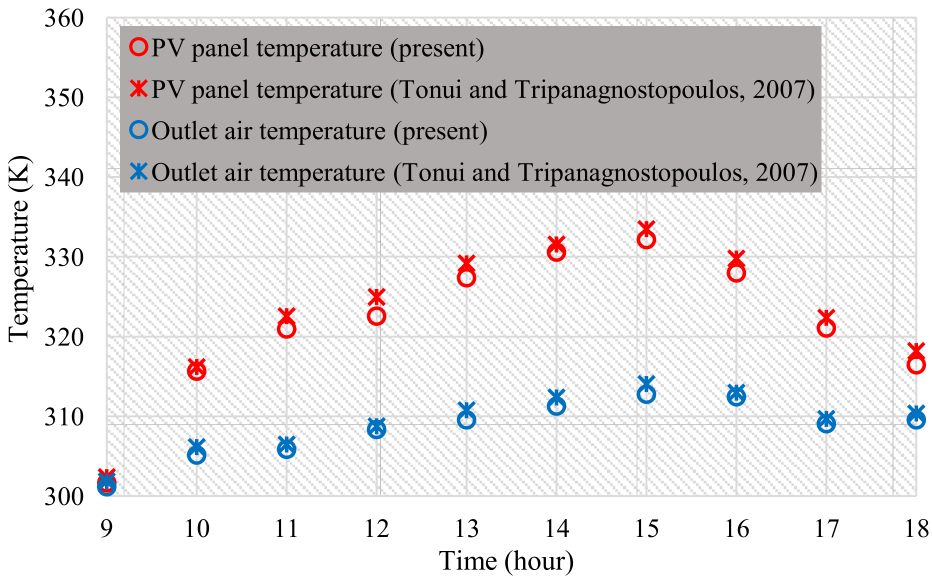

Fig. 5. Comparison between the findings of current assessment with those of Tonui and Tripanagnostopoulos (2007).

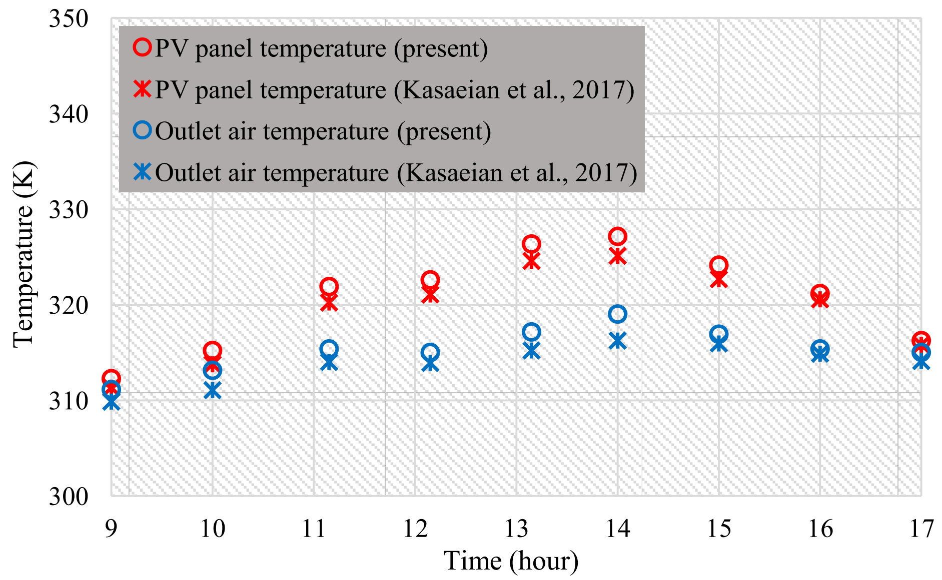

Fig. 6. Comparison between the findings of current assessment with those of Kasaeian et al. (2017).

4.2. Performance analysis

Fig. 7(a) depicts the hourly temperature of preheated air on the 15th of January. The figure also contains the hourly temperature of outdoor air to examine the amount of preheating at each hour. As is seen, the outlet air temperature is the same for both configurations, except from 8 AM to 16 PM. In other hours, the BIPVT collector is inactive, due to the zero radiation intensity, and there is no difference between the performances of different configurations of BIPVT-EAHE system. From 8 AM to 16 PM, the preheated air temperature in the configuration A is 0.47-4.4 °C higher than that of the configuration B and the maximum difference between the results of two configurations occurs at 12 AM. In January, because of the low ambient air temperature and solar radiation intensity, the increase in the temperature of the PV panels is less than the warm months of the year. Therefore, the increase in the air temperature by passing it through the channel located under the PV panels is not high. On the other hand, preheating the ambient air in the BIPVT system and then using it in the EAHE system leads to a reduction in the effectiveness of the EAHE system. These factors reduce the preheating performance of the configuration B compared to the configuration A in which the air first passes through the EAHE system, and then passes through the BIPVT system. Fig. 7(b) illustrates the hourly temperature of precooled air on the August 15th. Both configurations have a similar working principles in the cooling mode and consequently, there is no difference between their precooling results. It can be seen that the suggested system has a great performance in precooling the warm outdoor air. According to the results, the highest precooling of the outdoor air occurs at 3 PM, which is 13.34 °C.

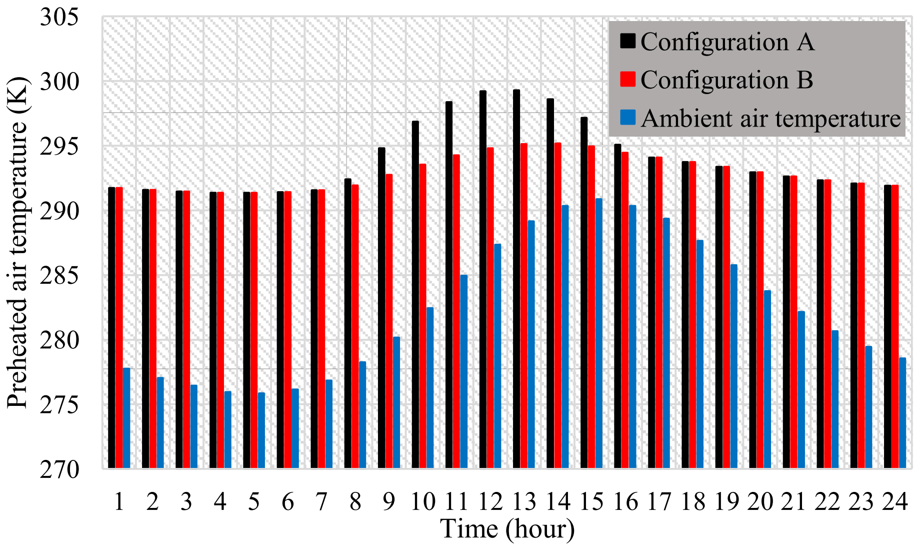

(a)

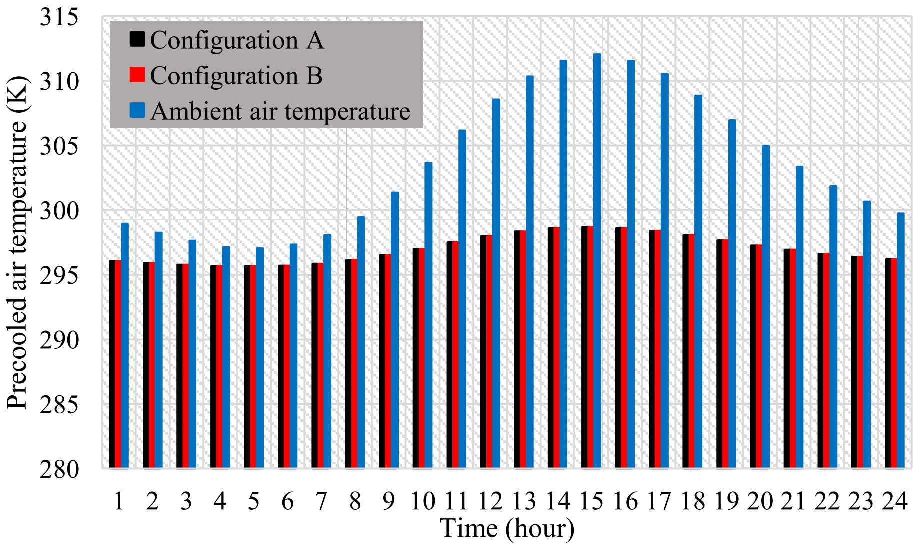

(b)

Fig. 7. Hourly temperature of preheated/precooled air for a (a) sample cold day (15th of January) and (b) sample warm day (15th of August).

The hourly temperature of PV module in two suggested configurations of the BIPVT-EAHE system are depicted in Fig. 8(a) and (b) for the January 15^{th} and August 15^{th}, respectively. It should be noted that the results presented in Fig. 8 are related to the hours at which solar radiation is available. During the studied cold day, the PV panel temperature in the configuration B is 3.63-14.13 °C lower than that of the configuration A, and therefore, the configuration B has a better performance in cooling the PV modules than the configuration A.

In the configuration A, the air passes through the EAHE system before passing under the modules, and gains heat. Thus, the cooling capacity reduces compared to the configuration B. Moreover, Fig. 8(b) shows that the configurations A and B have equal PV module temperatures during the sample warm day, which is because of the similar working principles of the cooling mode of these configurations.

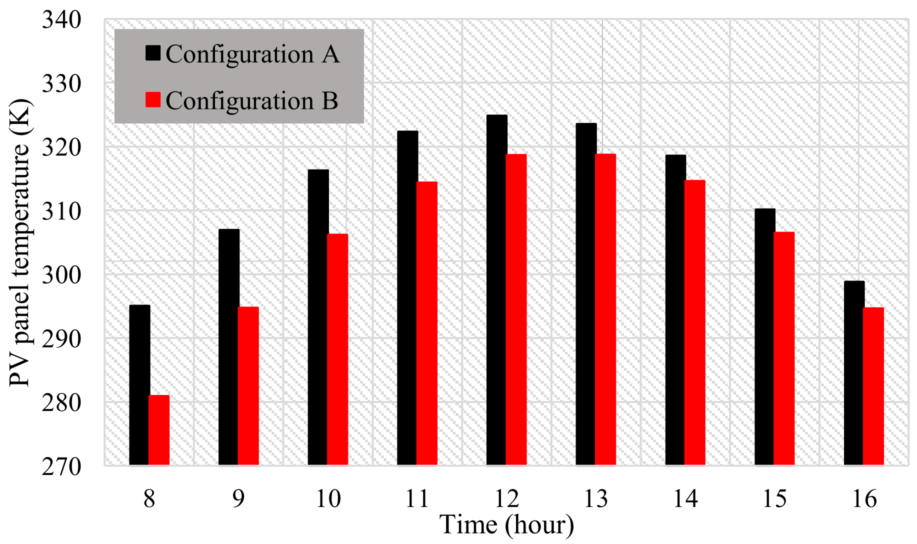

(a)

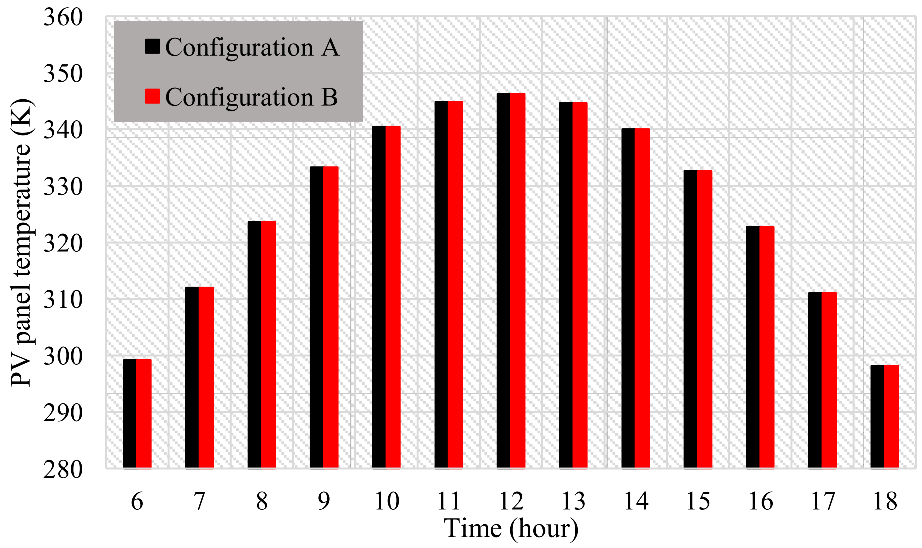

(b)

Fig. 8. Hourly temperature of PV module for a (a) sample cold day (January 15th) and (b) sample warm day (August 15th).

The monthly rate of received thermal energy by air from the two configurations of BIPVT-EAHE system is shown in Fig. 9. In the cooling mode, two configurations have the same performance; however, in the heating mode, except in March and October, the configuration A shows a better performance. During March and October, the ambient air temperature and the solar radiation intensity and, consequently, the PV panel temperature are more than the other cold months of the year. This makes the ambient air pre-heating through the BIPVT system more impressive than the EAHE system. Therefore, during these months, the configuration B represents a better performance than the configuration A, but with a decrease in both the ambient air temperature and solar radiation intensity, the opposite is true and the configuration A performs better than the configuration B. According to the results, the highest rate of thermal energy for both configurations occurs in January (493.62 and 449.63 kWh for configuration A and configuration B, respectively), while the lowest rate of thermal energy belongs to April (160.02 kWh for both configurations). The yearly rate of thermal energy recovered by the configurations A and B are 3499.59 and 3468.16 kWh, respectively.

Hence, it can be said that the configuration A has a slightly better heat transfer performance (0.91%) as compared with the configuration B.

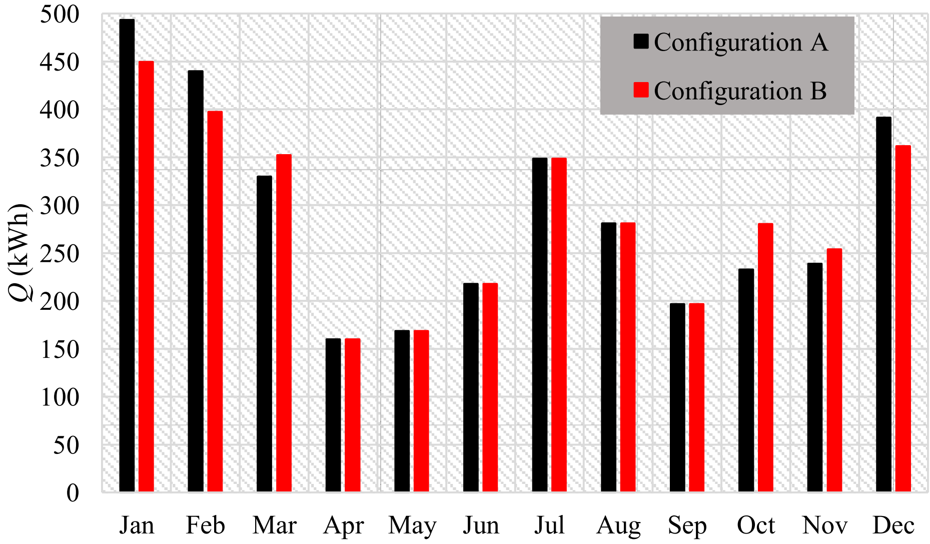

Fig. 9. The monthly thermal power gained from the different configurations of BIPVT-EAHE system

Fig. 10 shows the monthly electric power generated by the suggested configurations of BIPVT-EAHE system. The electricity produced by both configurations are equal in cooling mode; however, in the heating mode, the configuration B presents a better electrical performance compared to the configuration A. This is due to the lower temperature of the PV panels in configuration B in comparison with the configuration A. The maximum difference between the produced electricity in the heating mode of the two configurations occurs in January (4.79%). The yearly total electrical energy produced by the configurations A and B are respectively 5908.19 and 5969.87 kWh. Hence, it can be said that the electrical performance of the configurations B is slightly (1.04%) better than that of the configuration A.

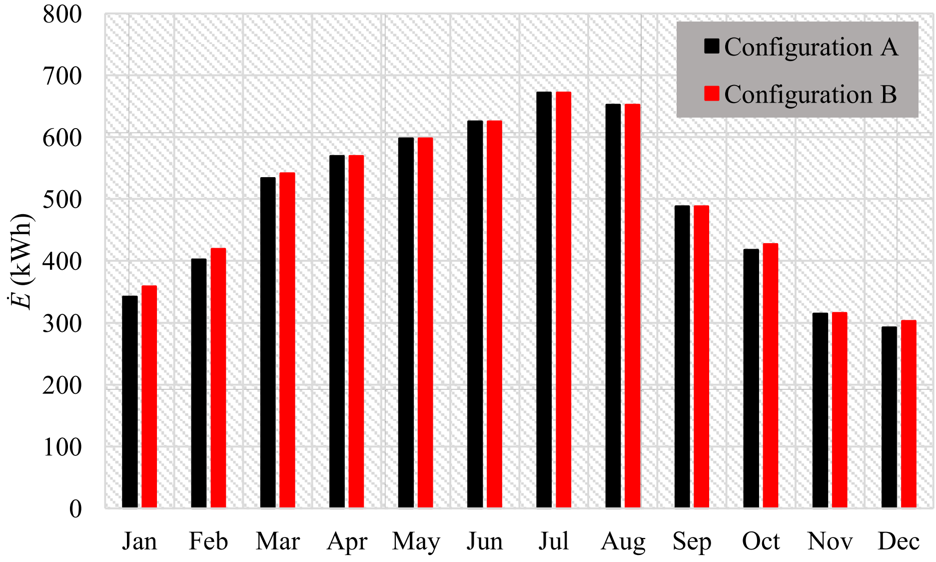

Fig. 10. The monthly electric power generated by the different configurations of BIPVT-EAHE system.

Fig. 11 gives the monthly rate of obtained thermal exergy from the different configurations of BIPVT-EAHE system. As shown, the performance of two configurations is the same in terms of thermal exergy in the cooling mode; however, in cold months, the thermal exergy obtained from the configuration A is better than the configuration B. The maximum difference between the generated rate of thermal exergy by configurations A and B is 19.75%, which occurs in February. The annual total rate of thermal exergy received from configuration A is 55.59 kWh, which is 7.39% higher than that of the configuration B (51.76 kWh).

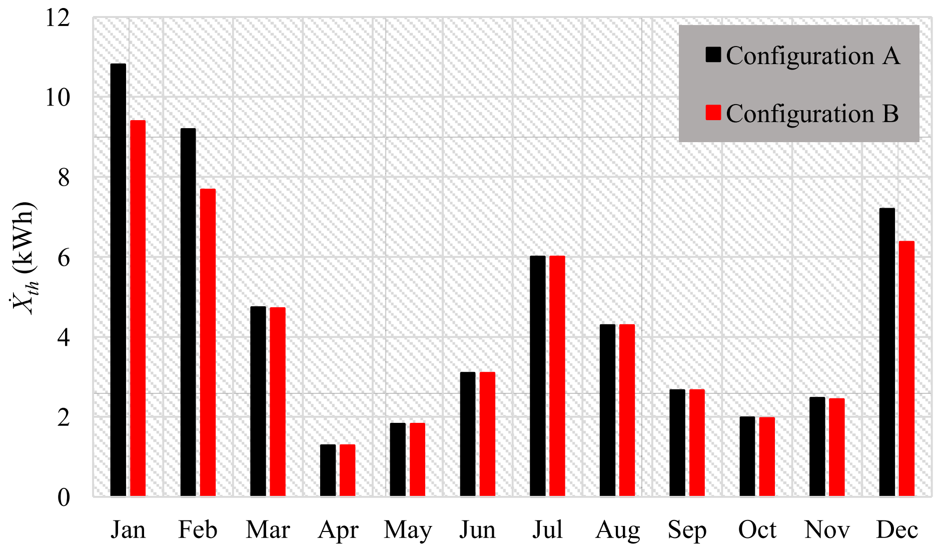

Fig. 11. The monthly rate of thermal exergy produced by the different configurations of BIPVT-EAHE system.

Fig. 12 shows the monthly average PEC_{en} of two configurations of BIPVT-EAHE system. The results show that the energy performance of both configurations are equal in the cooling mode; however, in the heating mode, except in December, the configuration B has a better energy performance than the configuration A. The maximum and minimum values of PEC_{en} of both configurations occurs in May (5.91 for configuration A and 6.05 for Configuration B) and January (2.48 for configuration A and 2.49 for configuration B), respectively. The yearly average PEC_{en} of configurations A and B are respectively 5.81 and 5.85, which indicates that the overall energy performance of configuration B is slightly (0.46%) better than the configuration A. In addition, in Fig. 12, it can be seen that PEC_{en} of both configurations in all months of the year is more than one, which shows that both configurations can provide the required total thermal load of the building.

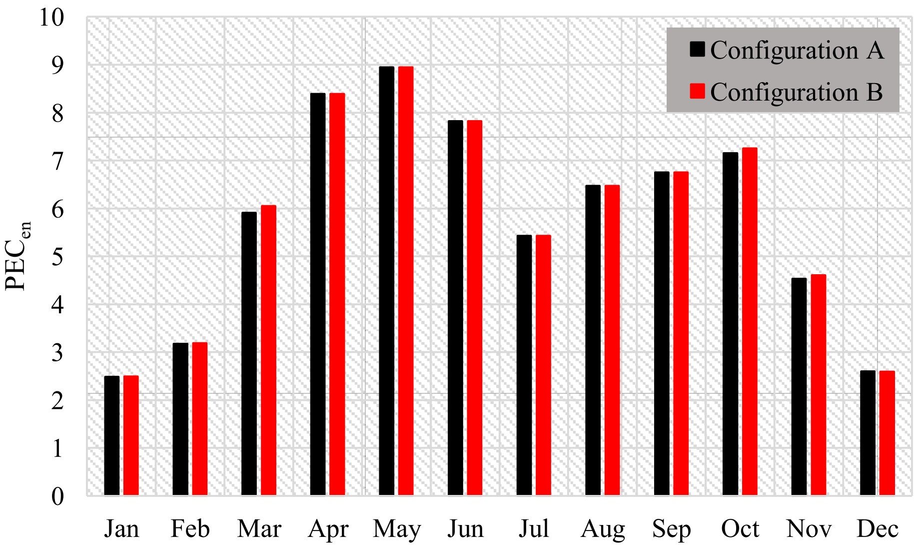

Fig. 12. The monthly average PEC$_{en}$ for different configurations of BIPVT-EAHE system.

The monthly average PEC$_{ex}$ of two configurations of PVT-EAHE system are demonstrated in Fig. 13. The exergy performance of both configurations are equal in the cooling mode; however, in the heating mode, except in October, the configuration B has a better exergy performance than the configuration A. The best exergy performance of both configurations occurs in April, while the worst one occurs in January. The yearly average PEC$_{ex}$ of the configuration A and configuration B is 121.14 and 121.51, respectively, and so it can be said that from the viewpoint of the second law of thermodynamics, the configuration A is slightly (0.02%) better than the configuration B.

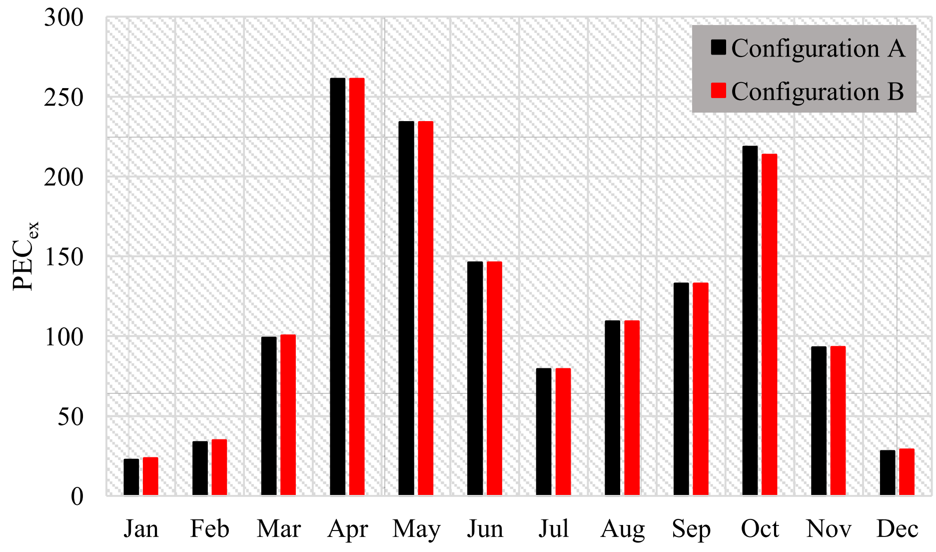

Fig. 13. The monthly average PEC_{ex} for different configurations of BIPVT-EAHE system.

At the end of this section, to better compare the performance of the configurations A and B, the results presented in this section are also tabulated in Table 2.

Table 2. Performance metrics of the different configurations of the BIPVT-EAHE system.

Month	Configuration A					Configuration B				
	$\dot{Q}$ (kWh)	$\dot{E}$ (kWh)	$\dot{Q}$ (kWh)	PEC_{en}	PEC_{ex}	$\dot{Q}$ (kWh)	$\dot{E}$ (kWh)	$\dot{Q}$ (kWh)	PEC_{en}	PEC_{ex}
Jan.	493.62	342.20	10.81	2.49	22.62	449.63	358.60	9.40	2.49	23.58
Feb.	439.80	402.30	9.19	3.18	33.62	397.31	419.14	7.68	3.19	34.87
Mar.	329.97	533.97	4.74	5.91	99.10	352.41	541.50	4.72	6.05	100.48
Apr.	160.02	569.45	1.29	8.39	261.23	160.02	569.45	1.29	8.39	261.23
May.	168.61	597.84	1.83	8.95	234.18	168.61	597.84	1.83	8.95	234.18
Jun.	217.78	625.15	3.10	7.83	146.22	217.78	625.15	3.10	7.83	146.22
Jul.	348.67	671.78	6.00	5.43	79.48	348.67	671.78	6.00	5.43	79.48
Aug.	281.20	652.23	4.29	6.48	109.24	281.20	652.23	4.29	6.48	109.24
Sep.	196.70	488.03	2.67	6.76	132.95	196.70	488.03	2.67	6.76	132.95
Oct.	232.94	417.56	1.99	7.15	218.61	280.34	427.38	1.97	7.25	213.60

Nov.	238.78	315.03	2.47	4.54	93.03	253.88	315.90	2.44	4.61	93.28
Dec.	391.49	292.65	7.20	2.60	28.15	361.62	302.87	6.37	2.60	29.03

4.3. Case study

In this section, the impacts of PVT and EAHE parameters on the annual average PEC_{en} and PEC_{ex} of the configuration B are examined. Fig. 14 illustrates the effect of duct length on the annual average PEC_{en} and PEC_{ex} of the configuration B at different duct widths. It is clear that both the annual average PEC_{en} and PEC_{ex} increase by boosting the duct length and duct width. Increasing the duct length results in a higher outlet air temperature and a higher pressure drop, which respectively increases and decreases the annual average PEC_{en} and PEC_{ex}. The results show that the effect of increasing the outlet air temperature is more pronounced, and as a result, the annual average PEC_{en} and PEC_{ex} enhance with intensifying the duct length. The increase in the duct width results in the following consequences:

- Reducing the air velocity which leads to an enhancement in the outlet air temperature and therefore, increases the rate of thermal energy and exergy of the system.
- Reducing the power consumption of fans due to a reduced pressure drop.
- Reducing the produced power of PV modules because of an enhancement in their temperature.
- Increasing the exposure area of the PV modules and consequently, increasing their production capacity.

Generally, the produced power of PV modules enhances with increasing the duct width. Higher values of the annual average PEC_{en} and PEC_{ex} by increasing the duct width shows that the effect of increase in the thermal energy, thermal exergy and produced power of the PV modules outweighs the impact of increase in the fan power consumption.

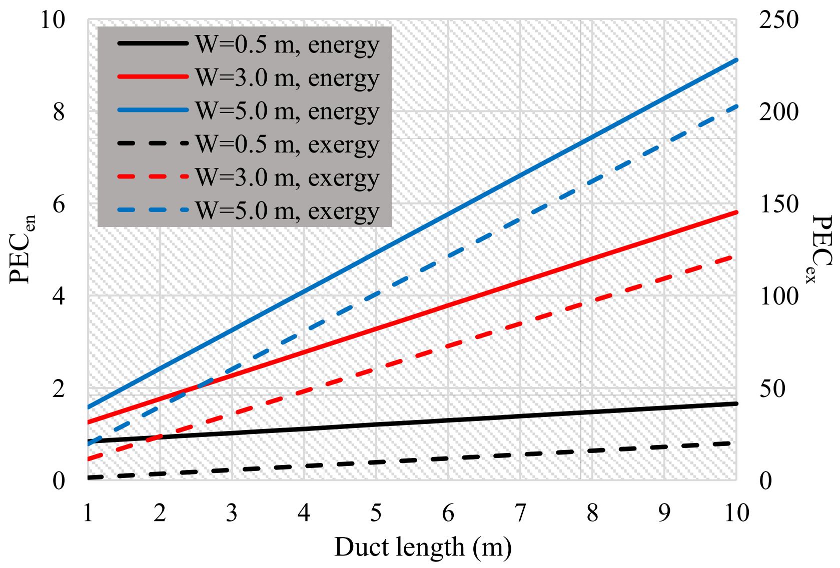

Fig. 14. The variation of yearly average PEC$_{en}$ and PEC$_{ex}$ as a function of duct length for different duct widths for the configuration B of BIPVT-EAHE system.

Fig. 15 gives the impact of air mass flow rate on the annual average PEC$_{en}$ and PEC$_{ex}$ of the configuration B at different duct depths. It is observed that both parameters reduce for a higher air mass flow rate and duct depth. Augmenting the air mass flow rate directly causes an improvement in the rate of obtained thermal energy, according to Eqs. (27) and (28), and thermal exergy, according to Eqs. (48) and (49), from the system. In addition, rising the air mass flow rate reduces the preheated air temperature in the heating mode or increases the precooled air temperature in the cooling mode, resulting in a reduction in the rate of obtained thermal energy and exergy of the system. The findings show that the impact of air mass flow rate on the thermal energy and exergy of the system is greater than the effect of air temperature, and therefore, the rate of thermal energy and exergy gained from the system increases with boosting the air mass flow rate. Moreover, an increase in the air mass flow rate reduces the temperature of the PV modules and, as a result, increases the rate of electricity generated by the modules. In addition, the fan power increases for a higher air mass flow rate, which reduces the annual average PEC$_{en}$ and PEC$_{ex}$ of the system. The results presented in

Fig. 15 show that the impact of boosted fan power outweighs the effects of increased thermal energy, thermal exergy, and generated electricity by the PV modules and therefore, the annual average PEC_{en} and PEC_{ex} decreases with increasing the air mass flow rate. Increasing the duct depth results in a decrease in the air velocity and as a result, both the thermal energy and exergy of the system increase. In addition, increasing the duct depth leads to a reduced rate of electricity produced by the PV modules and the power consumption of fans. Consequently, according to Fig. 15, by increasing the duct depth, the effect of decreasing the produced electricity of the PV modules overcomes the impact of reducing the fan power and therefore, the annual average PEC_{en} and PEC_{ex} of the system augments with boosting the duct depth.

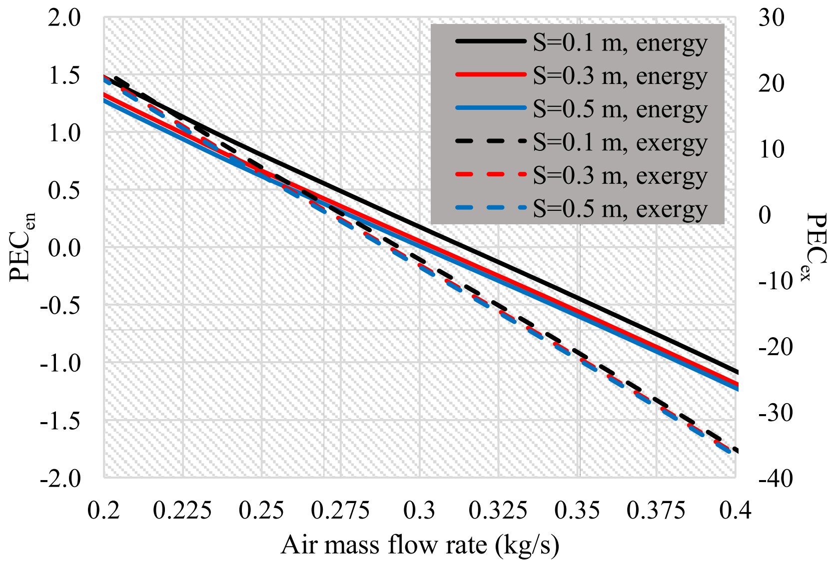

Fig. 15. The variation of yearly average PEC_{en} and PEC_{ex} as a function of air mass flow rate for different duct depths for the configuration B of BIPVT-EAHE system.

Fig. 16 depicts the influence of tube length of EAHE on the annual average PEC_{en} and PEC_{ex} of the configuration B at different tube diameters of EAHE system. The findings show that both the annual average PEC_{en} and PEC_{ex} increase with boosting the tube diameter.

Augmenting the tube diameter results in a higher effectiveness and therefore, higher rate of heat transfer in EAHE system. On the other hand, the air velocity reduces by increasing the tube diameter, which reduces the pressure drop and therefore, the fan power reduces by rising the tube diameter. Hence, the increased annual average PEC_{en} and PEC_{ex} of the configuration B with boosting the tube diameter is due to the increased rate of thermal energy/exergy and reduced fan power. Furthermore, Fig. 16 reveals that intensifying the pipe length in the tube diameters of 0.1 m and 0.5 m leads to a decrease in the annual average PEC_{en}; however, for the inner diameter of 0.3 m, it leads to an increase in the annual average PEC_{en}. Also, the results show that in the tube diameter of 0.1 m, the annual average PEC_{ex} decreases with increasing the tube length, while it is vice versa in the diameters of 0.3 m and 0.5 m. The increase in the pipe length leads to a higher rate of heat transfer in the EAHE system, resulting in a higher annual average PEC_{en} and PEC_{ex}. Besides, the pressure drop and hence, the fan consumed power augment with the increase in pipe length, which results in a lower annual average PEC_{en} and PEC_{ex}.

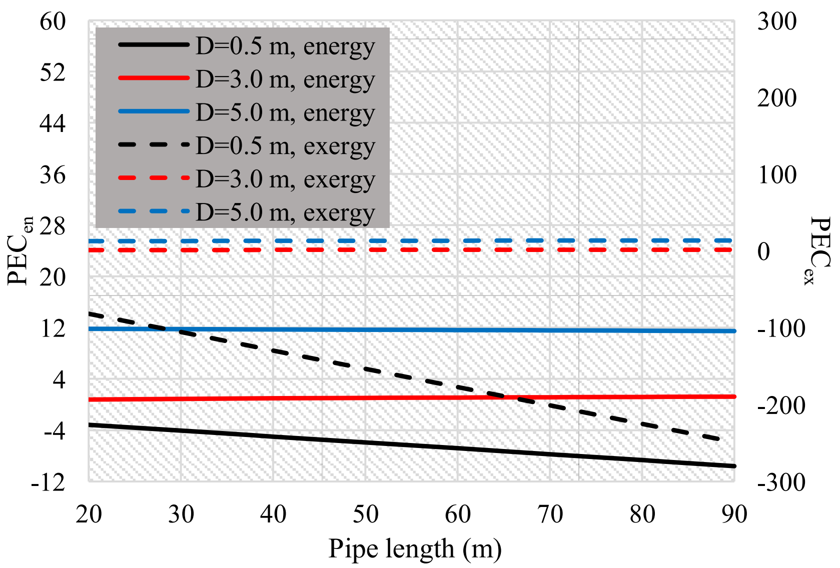

Fig. 16. The variation of yearly average PEC_{en} and PEC_{ex} as a function of pipe length for different inner pipe diameters of EAHE system for the configuration B of BIPVT-EAHE system.

5. Conclusion

In this study, two novel configurations of the BIPVT-EAHE system are proposed. Both configurations are capable of preheating/precooling the outdoor air in winter/summer and generating electricity. Besides, in both configuration, the building exhaust air is utilized to cool the PV modules. The hourly, monthly, and yearly energetic and exergetic aspects of both configurations are evaluated using an in-house Matlab code for Kermanshah weather conditions. In addition, the impacts of different influential parameters on the yearly average energetic and exergetic aspects of the best configuration of the BIPVT-EAHE system are examined. The following results are achieved from the study:

- The yearly rate of thermal energy, electrical energy, and thermal exergy gained from the configuration A are respectively 3499.59, 5908.19, and 55.59 kWh, while these values for the configuration B are respectively 3468.16, 5969.87, and 51.76 kWh.
- The yearly average PEC_{en} and PEC_{ex} of the configuration A are respectively 5.81 and 121.14, while these values for the configuration B are respectively 5.85 and 121.51. Therefore, the configuration B presents better energetic performance than the configuration A whereas the exergetic performance of the configuration A is better than the configuration B.
- Both the annual average PEC_{en} and PEC_{ex} of the BIPVT-EAHE system increase by boosting the duct length and duct width.
- Intensifying the air mass flow rate and duct depth results in a decrease in the annual average PEC_{en} and PEC_{ex} of the BIPVT-EAHE system.
- Both the annual average PEC_{en} and PEC_{ex} augment with enhancing the tube diameter of the EAHE system.

References

Agathokleous, R.A., Kalogirou, S.A., Karellas, S., 2018. Exergy analysis of a naturally ventilated Building Integrated Photovoltaic/Thermal (BIPV/T) system. Renewable Energy 128, 541-552.

Al-Ajmi, F., Loveday, D.L., Hanby, V.I., 2006. The cooling potential of earth–air heat exchangers for domestic buildings in a desert climate. Building and Environment 41, 235-244.

Al-Waeli, A.H.A., Sopian, K., Kazem, H.A., Chaichan, M.T., 2017. Photovoltaic/Thermal (PV/T) systems: Status and future prospects. Renewable and Sustainable Energy Reviews 77, 109-130.

Barbier, E., 1997. Nature and technology of geothermal energy: A review. Renewable and Sustainable Energy Reviews 1, 1-69.

Benemann, J., Chehab, O., Schaar-Gabriel, E., 2001. Building-integrated PV modules. Solar Energy Materials and Solar Cells 67, 345-354.

Bisoniya, T.S., Design of earth-air heat exchanger system. Geothermal Energy 3, 18.

Bojic, M., Trifunovic, N., Papadakis, G., Kyritsis, S., 1997. Numerical simulation, technical and economic evaluation of air-to-earth heat exchanger coupled to a building. Energy 22, 1151-1158.

Brogren, M., Nostell, P., Karlsson, B., 2001. Optical efficiency of a PV-thermal hybrid CPC module for high latitudes. Solar Energy 69, 173-185.

Chow, T.T., Hand, J.W., Strachan, P.A., 2003. Building-integrated photovoltaic and thermal applications in a subtropical hotel building. Applied Thermal Engineering 23, 2035-2049.

Chow, T.T., Chan, A.L.S., Fong, K.F., Lin, Z., He, W., Ji, J., 2009. Annual performance of building-integrated photovoltaic/water-heating system for warm climate application. Applied Energy 86, 689-696.

Chu, S., Cui, Y., Liu, N., 2016. The path towards sustainable energy. Nature Materils 16, 16.

De Paepe, M., Janssens, A., 2003. Thermo-hydraulic design of earth-air heat exchangers. Energy and buildings 35, 389-397.

Duffie, J.A., Beckman, W.A., 2013. Solar engineering of thermal processes: John Wiley & Sons.

IEA Online Data Services (https://www.iea.org/buildings/).

Jakhar, S., Soni, M.S., Boehm, R., 2018. Thermal Modeling of a Rooftop Photovoltaic/Thermal System With Earth Air Heat Exchanger for Combined Power and Space Heating, Journal of Solar Energy Engineering 140, 031011.

Jakhar, S., Soni, M.S., Gakkhar, N., 2016. Performance Analysis of Earth Water Heat Exchanger for Concentrating Photovoltaic Cooling. Energy Procedia 90, 145-153.

Jakhar, S., Soni, M.S., Gakkhar, N., 2017. Modelling and Simulation of Concentrating Photovoltaic System with Earth Water Heat Exchanger Cooling. Energy Procedia 109, 78-85.

Kasaeian, A., Khanjari, Y., Golzari, S., Mahian, O., Wongwises, S., 2017. Effects of Forced Convection on the Performance of a Photovoltaic Thermal System: An Experimental study. Experimental Thermal and Fluid Science 85, 13-21.

Khaki, M., Shahsavar, A., Khanmohammadi, S., Salmanzadeh, M., 2017. Energy and exergy analysis and multi-objective optimization of an air based building integrated photovoltaic/thermal (BIPV/T) system. Solar Energy 158, 380-395.

Khanmohammadi, S., Shahsavar, A., 2018. Energy analysis and multi-objective optimization of a novel exhaust air heat recovery system consisting of an air-based building integrated photovoltaic/thermal system and a thermal wheel. Energy Conversion and Management 172, 595-610.

Lund, J.W., Boyd, T.L., 2016. Direct utilization of geothermal energy 2015 worldwide review. Geothermics 60, 66-93.

Mahdavi, S., Sarhaddi, F., Hedayatizadeh, M., 2019. Energy/exergy based-evaluation of heating/cooling potential of PV/T and earth-air heat exchanger integration into a solar greenhouse, Applied Thermal Engineering 149, 996-1007.

Nayak, S., Tiwari, G.N., 2010. Energy metrics of photovoltaic/thermal and earth air heat exchanger integrated greenhouse for different climatic conditions of India. Applied Energy 87, 2984-2993.

Norton, B., Eames, P.C., Mallick, T.K., Huang, M.J., McCormack, S.J., Mondol, J.D., Yohanis, Y.G., 2011. Enhancing the performance of building integrated photovoltaics. Solar Energy 85, 1629-1664.

Prapas, D.E., Norton, B., Probert, S.D., 1987. Thermal design of compound parabolic concentrating solar-energy collectors. Journal of Solar Energy Engineering 109, 161-168.

Shahsavar, A., Khanmohammadi, S., Khaki, M., Salmanzadeh, M., 2018. Performance assessment of an innovative exhaust air energy recovery system based on the PV/T-assisted thermal wheel. Energy 162, 682-696.

Shahsavar, A., Rajabi, Y., 2018. Exergoeconomic and enviroeconomic study of an air based building integrated photovoltaic/thermal (BIPV/T) system. Energy 144, 877-886.

Shahsavar, A., Talebizadeh, P., Tabaei, H., 2013. Optimization with genetic algorithm of a PV/T air collector with natural air flow and a case study. Journal of Renewable and Sustainable Energy 5, 023118.

Tan, H., Charters, W., 1969. Effect of thermal entrance region on turbulent forced-convective heat transfer for an asymmetrically heated rectangular duct with uniform heat flux. Solar Energy 12, 513-516.

Tiwari, G.N., Meraj, M.D., Khan, M.E., Mishra, R.K., Garg, V., 2018. Improved Hottel-Whillier-Bliss equation for N-photovoltaic thermal-compound parabolic concentrator (N-PVT-CPC) collector, Solar Energy 166, 203-212.

Tiwari, G.N., Meraj, Khan, M.E., 2018. Exergy analysis of N-photovoltaic thermal-compound parabolic concentrator (N-PVT-CPC) collector for constant collection temperature for vapor absorption refrigeration (VAR) system. Solar Energy 173, 1032-1042.

Tonui, J., Tripanagnostopoulos, Y., 2007. Improved PV/T solar collectors with heat extraction by forced or natural air circulation. Renewable energy 32, 623-637.

Wu, J., Zhang, X., Shen, J., Wu, Y., Connelly, K., Yang, T., Tang L., Xiao, M., Wei, Y., Jiang, K., Chen, C., Xu, P., Wang, H., 2017. A review of thermal absorbers and their integration methods for the combined solar photovoltaic/thermal (PV/T) modules. Renewable and Sustainable Energy Reviews 75, 839-854.